haematologica
Journal of the Ferrata Storti Foundation

LSD1/KDM1A and GFI1B repress endothelial fate and induce hematopoietic fate in induced pluripotent stem cell-derived hemogenic endothelium

by Huan Zhang, Marten Hansen, Franca di Summa, Marieke von Lindern, Nynke Gillemans, Wilfred F.J. van IJcken, Arthur Flohr Svendsen, Sjaak Philipsen, Bert van der Reijden, Eszter Varga, and Emile van den Akker

Received: Feb 1, 2024.
Accepted: June 24, 2024.

Citation: Huan Zhang, Marten Hansen, Franca di Summa, Marieke von Lindern, Nynke Gillemans, Wilfred F.J. van IJcken, Arthur Flohr Svendsen, Sjaak Philipsen, Bert van der Reijden, Eszter Varga, and Emile van den Akker. LSD1/KDM1A and GFI1B repress endothelial fate and induce hematopoietic fate in induced pluripotent stem cell-derived hemogenic endothelium.
Haematologica. 2024 July 4. doi: 10.3324/haematol.2024.285214 [Epub ahead of print]

LSD1/KDM1A and GFI1B repress endothelial fate and induce hematopoietic fate in induced pluripotent stem cell-derived hemogenic endothelium.

Huan Zhang[1]*, Marten Hansen[1]*, Franca di Summa[1], Marieke von Lindern[1], Nynke Gillemans[2], Wilfred F.J. van IJcken[3], Arthur Flohr Svendsen[1], Sjaak Philipsen[2], Bert van der Reijden[4], Eszter Varga[1] and Emile van den Akker[1]

*equal contribution

[1]Department of Hematopoiesis, Sanquin Research and Landsteiner Laboratory, Amsterdam, The Netherlands.

[2]Department of Cell Biology, Erasmus MC, Rotterdam, The Netherlands.

[3]Center for Biomics, Erasmus MC, Rotterdam, The Netherlands.

[4]Department of Laboratory Medicine, Laboratory of Hematology, Radboud University Medical Center, Radboud Institute for Molecular Life Sciences, Nijmegen, The Netherlands.

Correspondence: Emile van den Akker, Department of Hematopoiesis, Sanquin Research, Plesmanlaan 125, 1066CX Amsterdam, The Netherlands; e-mail: e.vandenakker@sanquin.nl

Running title: LSD1/KDM1A and GFI1B control iPSC-derived EHT.

Acknowledgment:
The authors are grateful for the assistance provided by the Central Facility of Sanquin with flow cytometry and sorting.

Funding:
This work was supported by the Dutch Scientific Research organization (NWO) in the framework of the NWA-ORC Call grant agreement NWA.1160.18.038 (SYMPHONY), and by the ZonMw TRACER consortium as part of the PSIDER program (grant number 10250022110001).

Authorship:
Contributions: H.Z., M.H., and F.d.S. performed the experiments; H.Z., M.H., and E.v.d.A designed the experiments, analyzed the data, and wrote the manuscript; N.G. performed the RNA isolation and sequencing; H.Z., M.H., W.F.J.v.IJ., and A.S. analyzed the RNA sequencing data; M.v.L., S.P., B.v.d.R., and E.V. contributed to the experimental design and the writing of the manuscript. All authors critically revised the manuscript.

Conflict-of-interest disclosure:
The authors declare no conflicts of interest.

Data Sharing Statement:
For original data, please contact e.vandenakker@sanquin.nl. Sequencing data are available at GEO under the accession number GSE246386.

Abstract

Differentiation of induced pluripotent stem cells (iPSCs) into hematopoietic lineages offers great therapeutic potential. During embryogenesis, hemogenic endothelium (HE) gives rise to hematopoietic stem and progenitor cells through the endothelial-to-hematopoietic transition (EHT). Understanding this process using iPSCs is key to generating functional hematopoietic stem cells (HSCs), a currently unmet challenge. In this study, we examined the role of the transcriptional factor GFI1B and its co-factor LSD1/KDM1A in EHT. To this end, we employed patient-derived iPSC lines with a dominant negative dysfunctional GFI1B^{Q287*} and irreversible pharmacological LSD1/KDM1A inhibition in healthy iPSC lines. The formation of HE remained unaffected; however, hematopoietic output was severely reduced in both conditions. Single-cell RNA sequencing (scRNAseq) performed on the CD144^{+}/CD31^{+} population derived from healthy iPSCs revealed similar expression dynamics of genes associated with *in vivo* EHT. Interestingly, LSD1/KDM1A inhibition in healthy lines before EHT resulted in a complete absence of hematopoietic output. However, uncommitted HE cells did not display *GFI1B* expression, suggesting a timed transcriptional program. To test this hypothesis, we ectopically expressed GFI1B in uncommitted HE cells, leading to downregulation of endothelial genes and upregulation of hematopoietic genes, including *GATA2*, *KIT*, *RUNX1*, and *SPI1*. Thus, we demonstrate that LSD1/KDM1A and GFI1B can function at distinct temporal points in different cellular subsets during EHT. Although GFI1B is not detected in uncommitted HE cells, its ectopic expression allows for partial hematopoietic specification. These data indicate that precisely timed expression of specific transcriptional regulators during EHT is crucial to the eventual outcome of EHT.

Introduction

During human embryonic development, three spatiotemporally distinct waves of hematopoiesis occur[1]. Each wave exhibits different hematopoietic potencies. Yolk-sac primitive hematopoiesis produces primitive nucleated red blood cells, megakaryocytes, and macrophages[2]. The yolk sac also gives rise to erythroid myeloid progenitors (EMPs) that migrate to the fetal liver, generating the first definitive hematopoietic cells (*e.g.*, enucleated red blood cells)[3–5]. EMPs lack the potential to generate long-term hematopoietic stem cells (LT-HSCs) that provide lifelong hematopoietic support[5,6]. LT-HSCs arise in the intraembryonic aorta-gonad-mesonephros (AGM) region[7–10]. Both EMPs and HSCs derive from specialized endothelial cells, or hemogenic endothelium (HE), via a process termed endothelial-to-hematopoietic transition (EHT)[7–15]. However, human EHT remains ill-defined due to inaccessibility of primary material. Differentiation of human induced pluripotent stem cells (iPSCs) recapitulates certain aspects of embryonic development and provides a feasible model to study early hematopoiesis. Controlling AGM-like EHT from iPSCs *in vitro* would be a critical step toward generating an unlimited source of LT-HSCs for transplantation purposes and future *in vitro* blood production. So far, *in vitro* production of LT-HSCs from iPSCs has remained elusive, likely due to the absence of interactions with an inadequately defined niche and or the inability to capture the correct temporal hematopoietic wave[1]. Interestingly, subcutaneous administration of iPSCs into NOD-SCID mice results in teratoma formation, from which $CD34^+$ hematopoietic progenitor cells with long-term repopulating capacity can be isolated[16]. Thus, iPSC lines are intrinsically capable of generating LT-HSCs, but current protocols fail to achieve this *in vitro*. Additionally, long-term human hematopoietic reconstitution can be established in mice upon transplanting iPSC-derived HE with overexpression of seven transcription factors (ERG, HOXA5, HOXA9, HOXA10, LCOR, RUNX1, SPI1) [17]. Several other transitioning factors and regulators have also been implicated in playing a pivotal role in this process (GFI, GFI1B, RUNX1, GATA2)[18–22].

Runt-related transcription factor 1 (RUNX1) is a key factor in EHT[23]. Runx1 knockout mice are not viable after E12.5 due to a failure to establish adult hematopoiesis[24,25]. Growth factor independent 1 (GFI1) and growth factor independent 1B (GFI1B) are RUNX1's downstream targets. They function as transcriptional activators and repressors and share a DNA-binding motif (AATC)[26]. GFI1 and GFI1B exert their repressive function by recruiting transcriptional repressor complexes to their N-terminal SNAIL/GFI1 (SNAG) domain[27]. These complexes include lysine specific demethylase LSD1 (KDM1A), histone deacetylase 1 or 2 (HDAC1/2), and REST Corepressor CoREST (RCOR1)[28]. They replace active histone modifications with repressive marks, leading to the transcriptional repression of the endothelial program[29,30]. Furthermore, GFI1 and GFI1B can also activate specific genes independent of repressive co-factors recruitment[31].

Gfi1 knockout results in reduced HSC frequency, and Gfi1b-deficient mice do not develop after E14.5 due to defective erythropoiesis and megakaryopoiesis[18,19]. Deletion of their co-factor, *Lsd1/Kdm1a*, is

embryonically lethal (E5.5), while inducible knockdown showed that Lsd1/Kdm1a is essential for maintaining the HSC compartment in adult mice [32–36]. However, the precise function of GFI1B and LSD1/KDM1A on human EHT remains unclear. Although the role of combined overexpression of transcription factors in inducing EHT and trans-differentiation to hematopoietic cells has been studied, it is crucial to understand the contribution of each regulator individually to fully comprehend their role in emerging hematopoiesis from iPSC.

In this study, we aimed to decipher the molecular processes governing human iPSC-derived HE and EHT *in vitro* by manipulating GFI1B and its co-factor LSD1/KDM1A. We present a novel single-cell expression dataset from iPSC-derived HE undergoes EHT, revealing the kinetics of this process and offering insights into the underlying molecular mechanisms. Using a combination of patient-derived iPSC lines carrying a heterozygous mutation ($GFI1B^{Q287*}$) that introduces a stop codon within GFI1B's DNA binding site, inhibitors of LSD1/KDM1A (GSK-LSD1), and overexpression of GFI1B in iPSC-derived HE, we demonstrated that the loss of GFI1B and LSD1/KDM1A function does not impact the generation of HE. However, they are essential for the *in vitro* process of EHT in iPSCs.

Methods

iPSC culture and differentiation

iPSC lines (Supplementary method) were maintained on Matrigel (BD Biosciences) coated plates (TPP) in E8 medium (ThermoFisher Scientific) according to the manufacturer's instructions. Cells were incubated at 37^{o}C with 5% C02, passaged weekly, and differentiated as described previously[37]. Briefly, iPSCs were single-cell seeded on 6cm Matrigel coated plates with CloneR (StemCell Technologies) or Revitacell (ThermoFisher Scientific) and cultured for 8 days. When colonies reached a size of 400-600µm**,** differentiation was initiated by changing the medium to StemLineII (Sigma) supplemented with 50ng/ml bFGF (PeproTech), 40ng/ml VEGF (StemCell Technologies), 20ng/ml BMP4 (PeproTech), and insulin transferrin selenium (ITS, 1:100, ThermoFisher Scientific). At day 6, medium was changed to our homemade CellQuin[38] supplemented with 1:100 ITS, 10ng/ml VEGF, 20ng/ml BMP4, 10ng/ml IL-1β (StemCell Technologies), 1ng/ml IL-3 (StemCell Technologies), 10ng/ml IL-6 (StemCell Technologies), 50ng/ml TPO (StemCell Technologies), and 50ng/ml SCF (culture supernatant from 293T cells expressing ectopic SCF). Where indicated, 4µM GSK-LSD1 (Sigma) was added to cultures at day 5 or day 6 of iPSC differentiation. Differentiated cells were prepared for flow cytometry analysis at indicated days (Supplementary method; Supplementary Table 1).

EHT culture and transduction

Hemogenic endothelium (HE) was isolated via magnetic-activated cell sorting (MACS) using CD34 magnetic beads (Miltenyi Biotec). Following the published EHT culture protocol[17], these cells were maintained on Matrigel coated plates in serum-free media (StemSpan^{TM} SFEMII, StemCell Technologies) supplemented with 10µM ROCK inhibitor Y-27632 (StemCell Technologies), 5ng/ml bFGF, 10ng/ml BMP4, 5ng/ml VEGF, 50ng/ml SCF, 30ng/ml Nplate (Amgen), 10ng/ml FLT3 (StemCell Technologies), and 25ng/ml IGF1 (PeproTech).

293T cells were transfected with either the empty vector (EV) or GFI1B lentiviral construct (Supplementary method) along with psPAX2 (Addgene #12260) and VSV.G (Addgene #14888) plasmids using Polyethylenimine (PEI, Sigma). After transfection, virus supernatant was collected and applied to CD34^{+} HE cells. EHT media was refreshed one day post-transduction. Four days later, samples were digested using TrypLE Select (ThermoFisher Scientific) and prepared for analysis.

scRNAseq analysis

scRNAseq was performed at Single Cell Discoveries (Utrecht, The Netherlands) following standard 10× Genomics 3' V3.1 chemistry protocol. In brief, cells were rehydrated and loaded onto a 10× Chromium controller. Sequencing libraries were prepared following the standard 10× Genomics protocol and sequenced on the Illumina NovaSeq 6000 platform (read length: 150 bp, paired-end). Data analysis was performed with the R packages 'Monocle2' and 'Monocle3'[39–41]. Monocle2 was used for quality control;

cells with low or high reads (upper bound 1.3*SD and lower bound 0.3*SD) and mitochondrial contamination were discarded, yielding filtered data. For dimensional reduction, UMAP[42] was used with the following settings: PCA=10, umap.min_dist=0.35, and umap.n.neighbors=5. Cells were clustered using the Leiden algorithm (0.0001 resolution). Trajectory analysis was calculated after UMAP dimensional reduction with a minimal_brach_len of 30 and geodesic_distance_ratio of 1. Differentially expressed genes between clusters were identified using spatial autocorrection analysis, Moran's I, and linear regression model with negative binomial distribution, built within Monocle3[39–41]. Co-regulated genes were grouped into modules using Louvain community analysis[43] and used as inputs for cell type characterization using the Descartes cell types and tissue database.

Bulk RNAseq analysis

iPSC-derived HE cells were lentivirally transduced with either EV or GFI1B. RNA library was prepared as previously described[44] and sequenced on the Illumina HiSeq 2500 system. RNA sequencing reads were mapped to GRCh38 (hg38) using STAR. After removing low-quality reads, differential gene expression analysis was conducted using the glmLRT function embedded in the 'edgeR' package in R. We set log2 fold-change at 1 and false discovery rate (FDR) at 0.01.

Gene enrichment analysis

Gene enrichment analysis was conducted using the R package 'clusterProfiler'. Differentially expressed genes were ranked based on the log2 fold-change. These ranked lists were served as input for gene set enrichment analysis (GSEA). We used C2: curated gene sets, C8: Cell type signature gene sets, and molecular function (MF) subset of Gene Ontology (GO) gene sets from the Molecular Signatures Database (MSigDB) for GSEA.

Statistics

Statistical analysis was done using GraphPad Prism9 software. Mann-Whitney test or two-way ANOVA, followed by Tukey's multiple comparisons test, were performed. Significance p value cut-off was set at 0.05.

Results

An initial wave of CD144$^+$CD309$^+$ endothelial cells precedes the production of hematopoietic cells

To study EHT, we established the HE differentiation kinetics using three iPSC control lines obtained from healthy individuals[45,46] and differentiated them toward hematopoietic commitment using our previous established iPSC differentiation protocol (Fig. 1A)[37]. Cells with both endothelial and hematopoietic potential were defined by the co-expression of CD144 (VE-Cadherin) and CD309 (VEGFR2)[47,48]. A gradual decline of CD144$^+$CD309$^+$ cells within the differentiating colonies was observed, decreasing from 18% at day 6 (hematopoietic onset) to 3% at day 11 (Fig. 1B). To determine whether specification occurred in subsequent differentiation, we further distinguished the CD144$^+$CD309$^+$ population by expression of the endothelial marker CD73 (NT5E) and hematopoietic markers CD43 (SPN) /CD41 (ITGA2B) (Supplemental Figure 1A). Sorted CD144$^+$CD309$^+$CD73$^+$ cells were adherent cells with endothelial morphology, whereas sorted CD144$^+$CD309$^+$CD41$^+$ cells were suspension cells with blast/hematopoietic morphology. The initial wave of CD144$^+$CD309$^+$ cells was followed by an increase of CD43$^+$ hematopoietic cells in the supernatant (Fig. 1C). Hematopoietic suspension cells were distinguished by CD235$^+$ erythroid cells and CD41$^+$ megakaryocytic/hematopoietic progenitor cells (Fig. 1D, E). Although heterogeneity was observed between different iPSC lines, the overall differentiation kinetics were similar.

CD144$^+$CD309$^+$ cells intrinsically differentiate toward either endothelial or hematopoietic fate

We then explored whether CD144$^+$CD309$^+$ cells inherently differentiate into either hematopoietic or endothelial cells. We found that CD144$^+$CD309$^+$ cells express CD34, a marker associated with both cell types (Fig. 2A), Upon CD34$^+$ enrichment at day 5, before hematopoietic onset, we uncovered the presence of adhering CD144$^+$CD34$^+$CD31$^+$ cells (Fig. 2B). These cells were negative for CD73 (mature endothelial marker) and CD43 (hematopoietic marker). However, after an additional 4 days of culture, these cells further differentiated into either CD73$^+$ endothelial cells (68%) or CD43$^+$ hematopoietic cells (19%) with a small percentage (13%) remaining as CD43$^-$CD73$^-$ (Fig. 2C, D). These results suggest that once isolated, CD144$^+$CD309$^+$ cells are inherently primed to undergo specification into either hematopoietic or endothelial lineages.

GFI1B and LSD1/KDM1A are essential for hematopoietic specification during iPSC-EHT

Using the determined iPSC-HE differentiation kinetics as control, we set out to determine the role of GFI1B and LSD1/KDM1A during *in vitro* EHT from iPSC-HE. We employed two approaches: Firstly, we induced EHT in iPSC lines harbouring the GFI1B^{Q287*} dominant negative mutation[49,50]. Secondly, we pharmacologically inhibited LSD1/KDM1A (GSK-LSD1) at day 6 in control iPSC lines (Fig. 3A)[37,45,46,49,50]. Within the differentiating adherent cells of both GFI1B^{Q287*} and GSK-LSD1 conditions, the production, and kinetics of CD144$^+$CD309$^+$ cells were not affected (Fig. 3B). However, a significant decrease in hematopoietic commitment was observed, evidenced by the reduction of CD43$^+$ cells (Fig. 3C).

Concurrently, there was an increase in the $CD73^+$ endothelial population in both conditions (Supplemental Fig. 1B). Next, we examined the hematopoietic output, which comprises non-adherent blast cells harvested from the supernatant. In the supernatant fraction from both $GFI1B^{Q287*}$ and GSK-LSD1 treated conditions, there was a decline in cell yield (Supplemental Fig. 1C, D), and a noticeable decrease in the proportion of hematopoietic progenitors, as indicated by CD43 and CD41 expression (Fig. 3D). Within the reduced hematopoietic compartment, megakaryocytic commitment was drastically decreased in both conditions, as determined by CD41 and CD42 expression (Fig. 3E, F). Additionally, an almost complete absence of $CD235^+$ erythroid compartment was observed (Fig. 3G). The data indicate that GFI1B and LSD1/KDM1A are crucial modulators during iPSC-EHT and that the progression toward hematopoietic cells and specifically to the megakaryocytic and erythroid lineages depends on their function.

Single-cell RNA-sequencing reveals iPSC-HE and transitional stages to endothelial and hematopoietic cells

Our results suggest that LSD1/KDM1A and GFI1B play a key role in balancing $CD144^+CD309^+$ commitment toward either hematopoietic or endothelial fates. The specific stage at which LSD1/KDM1A and GFI1B exert their functions during iPSC-EHT remains unclear. To delve deeper into their role at the single cell level, we performed single-cell RNA sequencing (scRNAseq). A control iPSC line was differentiated and subsequently treated with a single pulse of GSK-LSD1 at day 5 [46]. We then sorted $CD144^+$ and $CD31^+$ cells at day 8, post hematopoietic commitment (Fig 4A). This allowed us to capture both the $CD43^+$ hematopoietic (18.40+/-5.16%) and $CD73^+$ endothelial (46.76+/-11.88%) commitment (Supplemental Fig. 1E). UMAP dimensional reduction revealed five major distinct cell populations, clusters I and II (endothelial), III (hematopoietic), IV (neuronal), and V (lymphoid), with potential transition stages between clusters I-II-III (Fig. 4B). We grouped differentially expressed genes into modules (Supplemental Fig. 2A, B) and used genes from each module to determine cell identity (Supplemental Table 2A). Through this methodology, we pinpointed a total of 11 modules, where genes from modules 3, 5, 8, 9, 10, and 11 reflected the cluster identity (Supplemental Fig. 2A, B; Supplemental Table 2B). We performed differential gene expression using linear regression model followed by gene set enrichment analysis (GSEA) between clusters II and III, which showed downregulation of hematopoietic and upregulation of endothelial signatures in cluster II (Fig. 4C; Supplemental Table 2C, D). We also noticed an enriched hematopoietic stem cell signature in cluster II (Supplemental Fig. 2C; Supplemental Table 2E). Comparing cluster II to cluster I, GSEA showed upregulation of hematopoietic and downregulation of endothelial signatures in cluster II (Supplemental Fig. 2D; Supplemental Table 2F, G). Together, these steps characterized cluster II as iPSC-HE. Top markers from each cluster aligned with the identified cell types (Fig. 4D; Supplemental Fig. 3 and Fig. 4). Lymphoid markers *CD3* and *CD7* were exclusively found in the lymphoid cluster (V; Supplemental Fig. 3 and Fig. 4). An embryonic and neuronal specific transcription factor, *SOX2*, and a central nervous system specific receptor protein tyrosine phosphatase, *PTPRZ1*, were uniquely expressed in the neuronal cluster (IV; Supplemental Fig. 3 and Fig. 4). The

endothelial cluster (I) displayed high expression of *TGFB* and its downstream target, *HAND1*, suggesting an endothelial-to-mesenchymal transition of cultured endothelial cells from iPSCs (Fig. 4D; Supplemental Fig. 3 and Fig. 4)[51]. This could elucidate the significant enrichment of genes encoding cell adhesion and extracellular matrix proteins, including *COL3A1*, *FN1*, *ITGA1*, *IGFBP3*, *IGFBP7*, and *LUM* (Fig. 4D; Supplemental Fig. 3 and Fig. 4)[51,52]. *CD73* was predominantly detected in the endothelial cluster (I; Fig. 4D), while hematopoietic markers, such as *CD43*, *CD41*, and *CD235*, along with transcription factors *KLF1*, *SPI1*, *GATA1*, *GATA2*, *RUNX1*, *GFI*, and *GFI1B*, were confined to the hematopoietic cluster (III; Fig. 4D; Supplemental Fig. 3 and Fig. 4). The expression of *CD144*, *CD31*, *CD309*, *CD34*, and other known arterial/hemogenic endothelial markers such as *GJA4*, *SOX17*, *DLL4*, and *CD40*, were specifically enriched in the iPSC-HE cluster (II; Fig. 4D; Supplemental Fig. 3 and Fig. 4)[48,53,54]. Thus, our scRNAseq data revealed iPSC-HE, committed hematopoietic and endothelial cells, and their transition states.

Trajectory analysis reveals gene regulation dynamics during iPSC-EHT

Next, we conducted a trajectory analysis to better understand the differentiation process. By designating the endothelial population as the originating node (cluster I, Fig. 4B), we computed and established the dynamics of similarity in pseudotime (Fig. 5A). Notably, the trajectory linking the iPSC-HE to both the hematopoietic and the endothelial clusters showed a reduction in the number of cells during transitional phases. This reduction was especially profound during the hematopoietic transition state, suggesting limited cellular proliferation during this phase. The pseudotime trajectory also allowed us to plot transcript abundance from iPSC-HE through iPSC-EHT to hematopoietic committed cells. We focused on the transcripts associated with *in vivo* AGM-EHT, including *NOTCH1*, *DLL4*, *HOXA5*, *HOXA9*, *ERG*, *LCOR*, *GATA2*, *RUNX1*, *SPI1*, *GFI1*, and *GFI1B* (Fig. 5B; Supplemental Fig. 5A, B). The expression of *NOTCH1* and its ligand, *DLL4*, increased in iPSC-HE and decreased during iPSC-EHT (Fig. 5B; Supplemental Fig. 4). This trend was followed by the upregulation of hematopoietic transcription factors such as *GATA2*, *RUNX1*, *GFI1*, and *GFI1B* (Fig. 4D; Fig. 5B; Supplemental Fig. 4). While *GFI1B* expression was not detected in iPSC-HE, it was upregulated during iPSC-EHT following the upregulation of *GATA2* and *RUNX1*. *LSD1*/*KDM1A*, a co-factor of GFI1B, was ubiquitously expressed (Fig. 5C; Supplemental Fig. 5C). Other known co-factors of GFI1B, such as *RCOR1*, *HDAC1*, and *HDAC2*, were also present in the iPSC-HE (Fig. 5C; Supplemental Fig. 5C). The trajectory analysis unveiled gene expression dynamics during EHT, pinpointing the absence of *GFI1B* in iPSC-HE and ubiquitous expression of *LSD1/KDM1A*.

LSD1/KDM1A is essential for EHT of iPSC-HE and is involved in endothelial differentiation

Next, we assessed the impact of GFI1B's co-factor LSD1/KDM1A on iPSC-HE specification toward hematopoietic or endothelial lineages through inhibition using GSK-LSD1. Inhibition of LSD1/KDM1A resulted in the absence of the hematopoietic cluster (Fig. 6A, B; Supplemental Fig. 6). This finding aligns with the suppression of hematopoietic commitment by GSK-LSD1 as shown in Figure 3. At the same time, LSD1/KDM1A inhibition did not impede differentiation into the endothelial lineage (Fig. 6B; Supplemental

Fig. 6). This was also validated by the expression of endothelial markers using flow cytometry (Supplemental Fig. 1B). However, the endothelial populations differentiated in the presence or absence of GSK-LSD1 did not fully overlap (Fig. 6A), suggesting that LSD1/KDM1A inhibition also influences the gene expression program during endothelial differentiation/specification. In summary, our scRNAseq data demonstrated that LSD1/KDM1A inhibition results in an early block of EHT preceding the evident expression of *GFI1B*. This indicates that while the phenotypes of GFI1B^{Q287*} mutation and GSK-LSD1 might appear similar based on marker expression, they likely can exert their effects at different cellular states.

Ectopic expression of GFI1B in HE suppresses endothelial and activates hematopoietic programs

Considering that LSD1/KDM1A is a co-factor of GFI1B, and its inhibition leads to a block of EHT, we hypothesized that the ectopic expression of GFI1B in iPSC-HE might result in a converse effect, specifically reinforcing the hematopoietic fate and downregulating the endothelial gene expression profile. We generated an additional scRNAseq dataset from the same experiment but at day 5 (prior to hematopoietic or endothelial specification) of differentiation and integrated it with the day 8 scRNAseq dataset (Supplemental Fig. 7A). We observed a ubiquitous expression of *LSD1/KDM1A*, whereas *GFI1B* was not detected prior to hematopoietic commitment (Supplemental Fig. 7B). We then lentivirally transduced GFI1B into day 5 sorted CD34$^+$CD144$^+$CD31$^+$CD43$^-$CD73$^-$ cells (Fig. 7A) and allowed them to differentiate further into CD73$^+$ endothelial or CD43$^+$ haematopoietic cells. More than 95% of the cells were GFP positive 5 days after transduction (Supplemental Fig. 7C). GFI1B ectopic expression led to an increase in the total number of cells and in the number of CD73$^+$ cells (Supplemental Fig. 7D, E). Flow cytometry revealed a reduction in the endothelial marker CD73 and a slight decrease in the haematopoietic marker CD43 expression (Fig. 7A, B). We then investigated transcriptional differences between the two groups using bulk RNA-sequencing. Principal component (PC) analysis showed a clear segregation of the GFI1B overexpressed conditions from the empty vector controls (Supplemental Fig. 8A), with PC1 explaining 76% of the variance. We identified 846 upregulated and 446 downregulated genes in the GFI1B overexpressed samples (Fig. 7C; Supplemental Table 3A). As expected, *GFI1B* was among the top 10 differentially expressed genes (Supplemental Fig. 8B; Supplemental Table 3A). Gene ontology terms related to cell cycle were significantly upregulated, aligning with the increased cell numbers (Supplemental Fig. 7D; Supplemental Table 3B). Gene set enrichment analysis manifested a potent reduction of the endothelial signature and a robust upregulation of the hematopoietic signature (Fig. 7D; Supplemental Table 3C). Upregulated genes included *GATA2*, *RUNX1*, *KIT*, *CD43*, while downregulated genes comprised *CD73*, *SOX6*, *SOX14*, and *SOX17* (Supplemental Fig. 8C; Supplemental Table 3A). *HOXA9* and *HOXA10* were lowly expressed, while *HOXA5* remained undetected (Supplemental Fig. 8C). *GFI1*, on the other hand, was decreased by GFI1B overexpression (Supplemental Fig. 8C). Consequently, GFI1B overexpression promotes a hematopoietic program at the expense of an endothelial program, even before the onset of *RUNX1* and *GATA2* expression.

Discussion

Thus far, attempts to derive long-term repopulating hematopoietic stem cells or effector cells from iPSC differentiation *in vitro* have been unsuccessful. *In vivo*, definitive hematopoiesis requires an endothelial-to-hematopoietic transition (EHT) from the hemogenic endothelium (HE) in the aorta-gonad-mesonephros (AGM) region of the embryo. In this study, we examined how functional inhibition of GFI1B and LSD1/KDM1A impacts the generation of hematopoietic/endothelial progenitors (iPSC-HE) and the process of endothelial and hematopoietic transition (iPSC-EHT). We used patient-derived iPSC lines harboring a heterozygous mutation in GFI1B ($GFI1B^{Q287*}$) and inhibited LSD1/KDM1A in healthy iPSC lines using GSK-LSD1. Treatment of iPSCs differentiated toward the hematopoietic lineage with GSK-LSD1, or hematopoietic differentiation of $GFI1B^{Q287*}$ mutant iPSC, did not impair iPSC-HE formation. However, hematopoietic lineage commitment was profoundly impaired. Patients with heterozygous $GFI1B^{Q287*}$ mutation manifested thrombocytopenia[50], so it is unlikely that GFI1B/LSD1 inhibition blocks the proliferation of early hematopoietic progenitors. Indeed, although GFI1B deficient mice die prenatally E15 due to a severe defect in erythropoiesis and megakaryopoiesis, conditional deficiency for Gfi1b in adult mice allows HSCs to maintain self-renewal and multilineage differentiation capabilities despite increased levels of reactive oxygen species and loss of quiescence[55]. Of note, this hematopoietic ablation does lead to defects in erythropoiesis and megakaryopoiesis in adult mice [56], and a myeloid bias in iPSC differentiation[57]. Furthermore, LSD1 inhibition leads to expansion of human hematopoietic progenitors *in vitro*[58]. Treatment with GSK-LSD1 resulted in a complete absence of EHT from iPSC-HE and a subsequent lack of hematopoietic cells, indicating a crucial dependence of iPSC-derived hematopoiesis on LSD1/KDM1A. This finding aligns with previous research that showed Lsd1/LSD1 inhibition blocks EHT in *ex vivo* cultured mouse AGM explants and prevents embryoid body differentiation in both $RUNX1^{-}$ primitive and $RUNX1^{+}$ definitive hematopoiesis[35,59]. Additionally, these results corroborate the essential role of Lsd1's binding partner, Gfi1b (and Gfi1), in the emergence of hematopoietic cells from these isolated intra-aortic hematopoietic clusters[25,35]. Collectively, this indicates that iPSC-derived hematopoiesis similarly depends on LSD1/GFI1B. Interestingly, the block in hematopoietic commitment induced by GSK-LSD1 preceded the upregulation of *GFI1* and *GFI1B*. This suggests different and temporally distinct roles for LSD1/KDM1A during EHT, the first of which may not rely on GFI1B/GFI1. Our data illustrate that GFI1B and LSD1/KDM1A are crucial regulators of the hematopoietic commitment of iPSC-HE via EHT.

Through trajectory analysis in pseudotime, we confirmed that the expression of key EHT regulators during iPSC-EHT, such as *NOTCH1*, *RUNX1*, and *GFI1B*, shares similar kinetics to those of the *in vivo* EHT. Our data probably mimics extraembryonic definitive hematopoiesis given lack of *HOXA* expression[60]. Sugimura *et al*. compared iPSC-HE with fetal liver hematopoiesis in mice and humans and identified 9 genes differentially expressed and required for long-term repopulating HSPC capability, specifically *ERG, HOXA5, HOXA9, HOXA10, LCOR, RUNX1*, and *SPI1*[17]. Overexpression of these genes in iPSC-HE

followed by injection into mice led to long-term reconstitution, albeit low engraftment levels[17]. However, it remains unclear whether the ectopic expression of GFI1B alone in iPSC-derived HE can drive EHT in human hematopoiesis. While GFI1B primarily functions as a transcriptional repressor, ectopic expression in HE resulted in 846 upregulated and 446 downregulated genes, suggesting dual roles for GFI1B as both a transcriptional activator and repressor[31]. However, the precise relationship between these differentially expressed genes and GFI1B, whether direct or indirect, remains to be elucidated. Importantly, upregulated genes are enriched for hematopoietic specification, while downregulated genes are associated with endothelial specification. Notably, the hematopoietic transcription factors *RUNX1* and *GATA2* were among the upregulated genes. GFI1B is recognized as a downstream target of RUNX1. In mouse embryonic stem cells that lack Runx1, Gfi1b aids in differentiation toward hematopoietic cells during EHT by suppressing endothelial and promoting hematopoietic programs[61]. A recent study observed diminished *Gfi1b* expression in *Gata2*$^{+/-}$ mice HSCs and demonstrated Gfi1b's capacity to restore embryonic HSCs in *gata2b*$^{-/-}$ zebrafish[22]. Our dataset also suggests that GFI1B can function both upstream and downstream of RUNX1 and GATA2 during iPSC-EHT, directing HE to the hematopoietic fate. We observed a decrease in *GFI1* expression by forced GFI1B overexpression, which agreed with previous finding that GFI1/GFI1B repress *GFI1* expression in human T cells[62]. We speculate that the reason why we did not observe an increased CD43 membrane expression might be due to the specific transcriptional regulation of CD43-associated proteins, which could be independent of GFI1B.

Purified iPSC-derived CD144^{+}CD31^{+}CD34^{+} cells tend to differentiate more toward the endothelial lineage than the hematopoietic lineage. Although these cells are non-committed, i.e., CD43^{-}CD73^{-}, a bias toward endothelial differentiation cannot be excluded. However, CD144^{+}CD31^{+}CD34^{+} cells, prior to specification, did not reveal any clearly separated populations based on RNA expression profiles (Supplemental Fig. 7A). Ectopic GFI1B expression suggests a conflicted state between differentiating into hematopoietic or endothelial lineages. Indeed, GFI1B expression in iPSC-HE by itself was insufficient to drive EHT but did provide a clear singular transcriptional program initiated by this transcription factor. It becomes important to perform similar experiments with other regulators of EHT, and by comparing our single-cell data to *in vitro* and *in vivo* studies of fetal hematopoiesis.

In conclusion, the roles of LSD1/KDM1A and GFI1B during *in vitro* EHT are critical for iPSC-derived hematopoiesis. While both the dominant-negative mutation of GFI1B (GFI1BQ287*) and LSD1/KDM1A inhibition obstruct EHT, LSD1/KDM1A can probably operate at distinct temporal points that are either dependent or independent on GFI/GFI1B and in different cellular subsets. Furthermore, ectopic expression of GFI1B in hemogenic endothelial cells results in the downregulation of endothelial genes and upregulation of hematopoietic genes. The precisely timed expression of specific transcriptional regulators during EHT appears to be important to the eventual outcome of EHT.

References:

1. Ivanovs A, Rybtsov S, Ng ES, et al. Human haematopoietic stem cell development: from the embryo to the dish. Development. 2017;144(13):2323-2337.
2. Palis J. Hematopoietic stem cell-independent hematopoiesis: emergence of erythroid, megakaryocyte, and myeloid potential in the mammalian embryo. FEBS Lett. 2016;590(22):3965-3974.
3. Palis J, Robertson S, Kennedy M, Wall C, Keller G. Development of erythroid and myeloid progenitors in the yolk sac and embryo proper of the mouse. Development. 1999;126(22):5073-5084.
4. Frame JM, McGrath KE, Palis J. Erythro-myeloid progenitors: “definitive” hematopoiesis in the conceptus prior to the emergence of hematopoietic stem cells. Blood Cells Mol Dis. 2013;51(4):220-225.
5. McGrath KE, Frame JM, Fegan KH, et al. Distinct Sources of Hematopoietic Progenitors Emerge before HSCs and Provide Functional Blood Cells in the Mammalian Embryo. Cell Rep. 2015;11(12):1892-1904.
6. Lassila O, Martin C, Toivanen P, Dieterlen-Lievre F. Erythropoiesis and Lymphopoiesis in the Chick Yolk-Sac-Embryo Chimeras: Contribution of Yolk Sac and Intraembryonic Stem Cells. Blood. 1982;59(2):377-381.
7. De Bruijn MFTR, Speck NA, Peeters MCE, Dzierzak E. Definitive hematopoietic stem cells first develop within the major arterial regions of the mouse embryo. EMBO J. 2000;19(11):2465-2474.
8. De Bruijn MFTR, Ma X, Robin C, et al. Hematopoietic stem cells localize to the endothelial cell layer in the midgestation mouse aorta. Immunity. 2002;16(5):673-683.
9. Medvinsky A, Dzierzak E. Definitive Hematopoiesis Is Autonomously Initiated by the AGM Region. Cell. 1996;86(6):897-906.
10. Ivanovs A, Rybtsov S, Welch L, et al. Highly potent human hematopoietic stem cells first emerge in the intraembryonic aorta-gonad-mesonephros region. J Exp Med. 2011;208(12):2417-2427.
11. Frame JM, Fegan KH, Conway SJ, McGrath KE, Palis J. Definitive hematopoiesis in the yolk sac emerges from Wnt-responsive hemogenic endothelium independently of circulation and arterial identity. Stem Cells. 2016;34(2):431-444.
12. Yoshimoto M, Porayette P, Glosson NL, et al. Autonomous murine T-cell progenitor production in the extra-embryonic yolk sac before HSC emergence. Blood. 2012;119(24):5706-5714.
13. Yoshimoto M, Montecino-Rodriguez E, Ferkowicz MJ, et al. Embryonic day 9 yolk sac and intra-embryonic hemogenic endothelium independently generate a B-1 and marginal zone progenitor lacking B-2 potential. Proc Natl Acad Sci U S A. 2011;108(4):1468-1473.
14. Boisset JC, Van Cappellen W, Andrieu-Soler C, et al. In vivo imaging of haematopoietic cells emerging from the mouse aortic endothelium. Nature. 2010;464(7285):116-120.
15. Lacaud G, Kouskoff V. Hemangioblast, hemogenic endothelium, and primitive versus definitive hematopoiesis. Exp Hematol. 2017;49:19-24.
16. Suzuki N, Yamazaki S, Yamaguchi T, et al. Generation of Engraftable Hematopoietic Stem Cells From Induced Pluripotent Stem Cells by Way of Teratoma Formation. Mol Ther. 2013;21(7):1424-1431.

17. Sugimura R, Jha DK, Han A, et al. Haematopoietic stem and progenitor cells from human pluripotent stem cells. Nature. 2017;545(7655):432-438.
18. Möröy T, Vassen L, Wilkes B, Khandanpour C. From cytopenia to leukemia: the role of Gfi1 and Gfi1b in blood formation. Blood. 2015;126(24):2561-2569.
19. Saleque S, Cameron S, Orkin SH. The zinc-finger proto-oncogene Gfi-1b is essential for development of the erythroid and megakaryocytic lineages. Genes Dev. 2002;16(3):301-306.
20. Tsai FY, Keller G, Kuo FC, et al. An early haematopoietic defect in mice lacking the transcription factor GATA-2. Nature. 1994;371(6494):221-226.
21. de Pater E, Kaimakis P, Vink CS, et al. Gata2 is required for HSC generation and survival. J Exp Med. 2013;210(13):2843-2850.
22. Koyunlar C, Gioacchino E, Vadgama D, et al. Gata2-regulated Gfi1b expression controls endothelial programming during endothelial-to-hematopoietic transition. Blood Adv. 2023;7(10):2082-2093.
23. North T, Gu TL, Stacy T, et al. Cbfa2 is required for the formation of intra-aortic hematopoietic clusters. Development. 1999;126(11):2563-2575.
24. Wang Q, Stacy T, Binder M, et al. Disruption of the Cbfa2 gene causes necrosis and hemorrhaging in the central nervous system and blocks definitive hematopoiesis. Proc Natl Acad Sci U S A. 1996;93(8):3444-3449.
25. Thambyrajah R, Patel R, Mazan M, et al. New insights into the regulation by RUNX1 and GFI1(s) proteins of the endothelial to hematopoietic transition generating primordial hematopoietic cells. Cell Cycle. 2016;15(16):2108-2114.
26. Anguita E, Villegas A, Iborra F, Hernández A. GFI1B controls its own expression binding to multiple sites. Haematologica. 2010;95(1):36-46.
27. Chiang C, Ayyanathan K. SNAIL/Gfi-1 (SNAG) Family Zinc Finger Proteins in Transcription Regulation, Chromatin Dynamics, Cell Signaling, Development, and Disease. Cytokine Growth Factor Rev. 2013;24(2):123-131.
28. Saleque S, Kim J, Rooke HM, Orkin SH. Epigenetic Regulation of Hematopoietic Differentiation by Gfi-1 and Gfi-1b Is Mediated by the Cofactors CoREST and LSD1. Mol Cell. 2007;27(4):562-572.
29. Zweidler-Mckay PA, Grimes HL, Flubacher MM, Tsichlis PN. Gfi-1 encodes a nuclear zinc finger protein that binds DNA and functions as a transcriptional repressor. Mol Cell Biol. 1996;16(8):4024-4034.
30. Duan Z, Horwitz M. Targets of the transcriptional repressor oncoprotein GFI-1. Proc Natl Acad Sci U S A. 2003;100(10):5932-5937.
31. Acar M, Jafar-Nejad H, Giagtzoglou N, et al. Senseless physically interacts with proneural proteins and functions as a transcriptional co-activator. Development. 2006;133(10):1979-1989.
32. Wang J, Scully K, Zhu X, et al. Opposing LSD1 complexes function in developmental gene activation and repression programmes. Nature. 2007;446(7138):882-887.
33. Sprüssel A, Schulte JH, Weber S, et al. Lysine-specific demethylase 1 restricts hematopoietic progenitor proliferation and is essential for terminal differentiation. Leukemia. 2012;26(9):2039-2051.

34. Takeuchi M, Fuse Y, Watanabe M, et al. LSD1/KDM1A promotes hematopoietic commitment of hemangioblasts through downregulation of Etv2. Proc Natl Acad Sci U S A. 2015;112(45):13922-13927.
35. Thambyrajah R, Mazan M, Patel R, et al. GFI1 proteins orchestrate the emergence of haematopoietic stem cells through recruitment of LSD1. Nat Cell Biol. 2015;18(1):21-32.
36. Wang J, Hevi S, Kurash JK, et al. The lysine demethylase LSD1 (KDM1) is required for maintenance of global DNA methylation. Nat Genet. 2008 41:1. 2008;41(1):125-129.
37. Hansen M, Varga E, Aarts C, et al. Efficient production of erythroid, megakaryocytic and myeloid cells, using single cell-derived iPSC colony differentiation. Stem Cell Res. 2018;29:232-244.
38. Heshusius S, Heideveld E, Burger P, et al. Large-scale in vitro production of red blood cells from human peripheral blood mononuclear cells. Blood Adv. 2019;3(21):3337-3350.
39. Trapnell C, Cacchiarelli D, Grimsby J, et al. The dynamics and regulators of cell fate decisions are revealed by pseudotemporal ordering of single cells. Nat Biotechnol. 2014;32(4):381-386.
40. Qiu X, Mao Q, Tang Y, et al. Reversed graph embedding resolves complex single-cell trajectories. Nat Methods. 2017;14(10):979-982.
41. Cao J, Spielmann M, Qiu X, et al. The single-cell transcriptional landscape of mammalian organogenesis. Nature. 2019;566(7745):496-502.
42. McInnes L, Healy J, Melville J. UMAP: Uniform Manifold Approximation and Projection for Dimension Reduction. arXiv. 2020 Sep 18. doi:10.48550/arXiv.1802.03426 [preprint, not peer-reviewed]
43. Blondel VD, Guillaume JL, Lambiotte R, Lefebvre E. Fast unfolding of communities in large networks. J Stat Mech. 2008;2008(10):P10008.
44. Heshusius S, Grech L, Gillemans N, et al. Epigenomic analysis of KLF1 haploinsufficiency in primary human erythroblasts. Sci Rep. 2022;12(1):336.
45. Hansen M, Varga E, Wüst T, et al. Generation and characterization of human iPSC lines SANi001-A and SANi002-A from mobilized peripheral blood derived megakaryoblasts. Stem Cell Res. 2017;25:42-45.
46. Hansen M, Varga E, Wüst T, et al. Generation and characterization of human iPSC line MML-6838-Cl2 from mobilized peripheral blood derived megakaryoblasts. Stem Cell Res. 2017;18:26-28.
47. Choi KD, Vodyanik MA, Togarrati PP, et al. Identification of the Hemogenic Endothelial Progenitor and Its Direct Precursor in Human Pluripotent Stem Cell Differentiation Cultures. Cell Rep. 2012;2(3):553-567.
48. Sturgeon CM, Ditadi A, Clarke RL, Keller G. Defining the path to hematopoietic stem cells. Nat Biotechnol. 2013;31(5):416-418.
49. Van Oorschot R, Hansen M, Koornneef JM, et al. Molecular mechanisms of bleeding disorderassociated GFI1BQ287* mutation and its affected pathways in megakaryocytes and platelets. Haematologica. 2019;104(7):1460-1472.
50. Hansen M, Varga E, Wüst T, et al. Generation and characterization of a human iPSC line SANi005-A containing the gray platelet associated heterozygous mutation p.Q287* in GFI1B. Stem Cell Res. 2017;25:34-37.

51. Wang H, Wang M, Wen Y, et al. Biphasic Regulation of Mesenchymal Genes Controls Fate Switches During Hematopoietic Differentiation of Human Pluripotent Stem Cells. Adv Sci. 2020;7(20):2001019.
52. Angelos MG, Abrahante JE, Blum RH, Kaufman DS. Single cell resolution of human hemato-endothelial cells defines transcriptional signatures of hemogenic endothelium. Stem Cells. 2018;36(2):206-217.
53. Zeng Y, He J, Bai Z, et al. Tracing the first hematopoietic stem cell generation in human embryo by single-cell RNA sequencing. Cell Res. 2019;29(11):881-894.
54. Pearson S, Lancrin C, Lacaud G, Kouskoff V. The sequential expression of CD40 and Icam2 defines progressive steps in the formation of blood precursors from the mesoderm germ layer. Stem Cells. 2010;28(6):1089-1098.
55. Khandanpour C, Sharif-Askari E, Vassen L, et al. Evidence that Growth factor independence 1b regulates dormancy and peripheral blood mobilization of hematopoietic stem cells. Blood. 2010;116(24):5149-5161.
56. Foudi A, Kramer DJ, Qin J, et al. Distinct, strict requirements for Gfi-1b in adult bone marrow red cell and platelet generation. J Exp Med. 2014;211(5):909-927.
57. Venhuizen J, van Bergen MGJM, Bergevoet SM, et al. GFI1B and LSD1 repress myeloid traits during megakaryocyte differentiation. Commun Biol. 2024;7(1):1-9.
58. Subramaniam A, Žemaitis K, Talkhoncheh MS, et al. Lysine-specific demethylase 1A restricts ex vivo propagation of human HSCs and is a target of UM171. Blood. 2020;136(19):2151-2161.
59. Bruveris FF, Ng ES, Leitoguinho AR, et al. Human yolk sac-like haematopoiesis generates RUNX1-, GFI1- and/or GFI1B- dependent blood and SOX17-positive endothelium. Development. 2020;147(20):dev193037.
60. Ng ES, Azzola L, Bruveris FF, et al. Differentiation of human embryonic stem cells to HOXA+ hemogenic vasculature that resembles the aorta-gonad-mesonephros. Nat Biotechnol. 2016;34(11):1168-1179.
61. Lancrin C, Mazan M, Stefanska M, et al. GFI1 and GFI1B control the loss of endothelial identity of hemogenic endothelium during hematopoietic commitment. Blood. 2012;120(2):314-322.
62. Doan LL, Porter SD, Duan Z, et al. Targeted transcriptional repression of Gfi1 by GFI1 and GFI1B in lymphoid cells. Nucleic Acids Res. 2004;32(8):2508-2519.

Fig.1. Hematopoietic commitment during iPSC differentiation. (A) Schematic overview of iPSC differentiation, specifying stages of induction, the growth factors used, and the differentiation timeline in days[37]. **(B)** Gating strategy to track hematopoietic/endothelial precursors during iPSC differentiation in culture dish-adherent colonies through assessing the expression of CD144 and CD309. The percentage of $CD144^+CD309^+$ cells from day 6 to 14 during differentiation is shown on the right (mean +/- SD; n=6-20). **(C)** Early hematopoietic commitment evaluated by the percentage of $CD43^+$ cells in suspension from day 7 to 14 during iPSC differentiation (mean +/- SD; n=6-21). **(D)** Percentage of $CD41^+$ megakaryocytic/hematopoietic progenitor cells and **(E)** $CD235^+$ erythroid cells in suspension at day 8, 11, and 14 of iPSC differentiation (mean +/- SD; n=8-12).

Fig.2. Culture and specification of sorted hematopoietic/endothelial precursors. (A) Proportion of $CD34^+$ cells within the $CD309^+CD144^+$ population from day 5 to day 9 during iPSC differentiation (mean +/- SD; n=5). **(B)** CD34 MACS-sorted hematopoietic/endothelial precursors on day 5 of iPSC differentiation, with a purity of 96.7% (top left, blue: unstained; red: CD34 staining), highly enriched for CD31 and CD144 (95.9%, top right), predominantly uncommitted or negative for CD43 and CD73 (85.2%). **(C)** The development of hematopoietic/endothelial cells upon sub-culturing of day 5 $CD34^+$ precursors, captured at intervals of 1-, 2-, 3-, and 4-days post-plating. Representative figures showing the morphological progression (scale bar: 200μm; red arrows indicate examples of the emerging hematopoietic cells). **(D)** Differentiation of day5 $CD34^+$ precursors into CD73+ endothelial (in blue circle) and CD43+ hematopoietic (in red square) cells at day 1 and day 4 after sub-culturing. Data represents mean (n=2).

Fig.3. LSD1/KDM1A and GFI1B are critical regulators governing EHT from iPSCs. (A) Schematic overview of iPSC differentiation detailing growth factors, induction stages, and the pulse addition of GSK-LSD1 over the timeline in days. **(B)** Colonies differentiated for 6-14 days were harvested and stained for CD144 and CD309. Frequency of cells double positive for these markers is shown (n=6-20 for control, 6-12 for $GFI1B^{Q287*}$, and 3-12 for GSK-LSD1). **(C)** Percentage of $CD43^+$ cells within the differentiated colonies (n=11-20 for control, 7-12 for $GFI1B^{Q287*}$, and 5-11 for GSK-LSD1). **(D)** Early hematopoietic commitment was evaluated by assessing the proportion of $CD43^+$ cells among suspension cells during the differentiation of iPSCs (n=17-21 for control, 11-16 for $GFI1B^{Q287*}$, and 9-15 for GSK-LSD1). **(E)** The frequency of $CD41^+$ megakaryocytic/early hematopoietic progenitors (n=8-12 for control, 4-7 for $GFI1B^{Q287*}$, and 9-12 for GSK-LSD1), **(F)** $CD42^+$ megakaryocytic (n=12 for control, 6 for $GFI1B^{Q287*}$, and 12 for GSK-LSD1) and **(G)** $CD235^+$ erythroid (n=8-12 for control, 4-7 for $GFI1B^{Q287*}$, and 9-12 for GSK-LSD1) among suspension cells during iPSC colony differentiation, in the absence or presence of GSK-LSD1, or in cultures of iPSCs carrying the $GFI1B^{Q287*}$ mutation. (**B-G)** Data represent mean +/- SD, analyzed using two-way ANOVA, Tukey's multiple comparisons test. Significance levels: * < 0.05, ** <0.005, *** <0.0005, **** <0.00005. Representations: Black circles = control iPSC; Red triangles = iPSC treated with GSK-LSD1 inhibitor; Purple squares = $GFI1B^{Q287*}$ iPSC.

Fig.4. Identification of $CD144^+/CD31^+$ populations using scRNAseq. (A) A schematic diagram illustrating the timeline of iPSC differentiation, specifying the growth factors, induction stages, and the pulse addition of GSK-LSD1. iPSC colonies differentiated by Day 8 were stained for CD144 and CD31, and cells positive for either one or both markers were sorted ($CD144^+/CD31^+$). **(B)** Identification of $CD144^+/CD31^+$ cell populations using UMAP dimensional reduction is displayed, with colors corresponding to the identified cell types. **(C)** Enrichment of hematopoietic cell types in cluster III (top plot) and endothelial cell types in cluster II (bottom plot) by gene set enrichment analysis (GSEA). **(D)** UMAP plots displaying the expression of hematopoietic genes (*GFI1B*, *GFI1*, *RUNX1*, *CD43*), HE-associated genes (*GJA4*, *CD144*, *CD34*), and endothelial-related genes (*TGFBI*, *FN1*, *CD73*).

Fig.5. Pseudotime gene expression analysis during iPSC-EHT. (A) UMAP visualization of cells along the pseudotime, with the inferred pseudotime represented by a color gradient from blue to red. **(B)** Expression of *NOTCH1*, *DLL4*, *GATA2*, *RUNX1*, *GFI1B*, and *GFI* over pseudotime. **(C)** Expression of GFI1B co-factorss, *LSD1/KDM1A*, *RCOR1*, *HDAC1*, and *HDAC2* over pseudotime.

Fig.6. GSK-LSD1 blocks iPSC-EHT. (A) UMAP visualization of single $CD31^{+}/CD144^{+}$ cells differentiated from an iPSC line derived from a healthy donor, displayed under both untreated control (black) and GSK-LSD1 treated conditions (red). **(B)** Proportional representation of hematopoietic, hemogenic endothelial (HE), and endothelial populations, presented in Figure 5B, under both control and GSK-LSD1 conditions (control: hematopoietic 0.324, HE 0.257, endothelial 0.419; GSK-LSD1: hematopoietic 0.015, HE 0.394, endothelial 0.591)**.**

Fig.7. GFI1B ectopic expression in iPSC-HE leads to upregulation of hematopoietic genes and downregulation of endothelial genes. (A) Flow cytometry analysis of the endothelial marker CD73 and the hematopoietic marker CD43 on day 0 and day4 following transduction with either empty vector (EV) or GFI1B. The percentages are indicated within the plot. **(B)** Comparison of Mean Fluorescence Intensity (MFI) of CD43 and CD73 on day 4 post-transduction between EV and GFI1B groups (n = 3; mean +/- SD; analyzed via the Mann-Whitney test; p = 0.1 for both). **(C)** Heatmap displaying differentially expressed genes between EV and GFI1B groups on day 4 following transduction. **(D)** Enrichment of hematopoietic cell types in GFI1B-overexpressed iPSC-HE (top plot) and endothelial cell types in EV (bottom plot) by gene set enrichment analysis (GSEA).

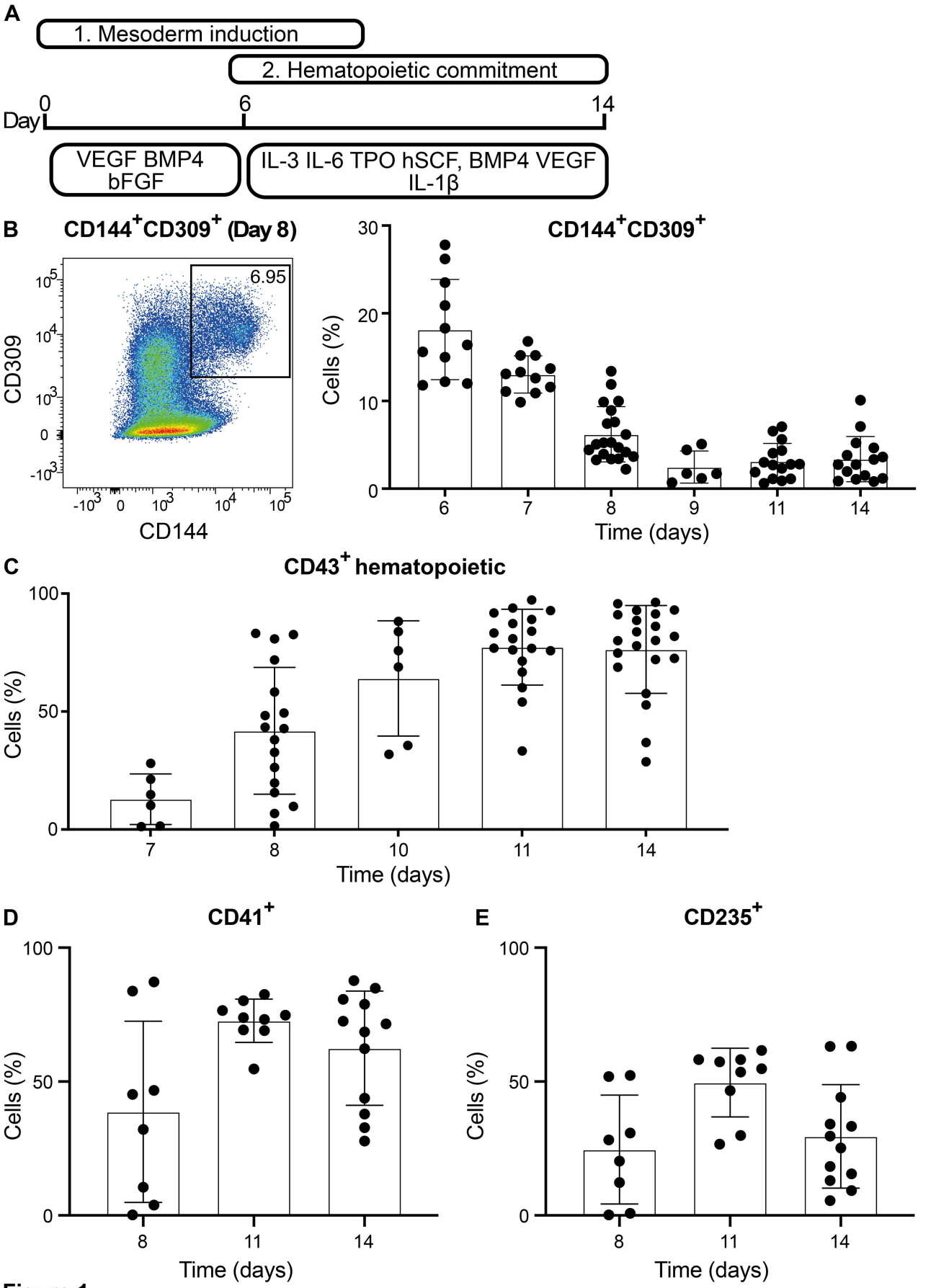
A
1. Mesoderm induction
2. Hematopoietic commitment
Day
0
6
14
VEGF BMP4 bFGF
IL-3 IL-6 TPO hSCF, BMP4 VEGF IL-1β
B
CD144+CD309+ (Day 8)
6.95
CD309
CD144
CD144+CD309+
Cells (%)
Time (days)
C
CD43+ hematopoietic
Cells (%)
Time (days)
D
CD41+
Cells (%)
Time (days)
E
CD235+
Cells (%)
Time (days)

Figure 1

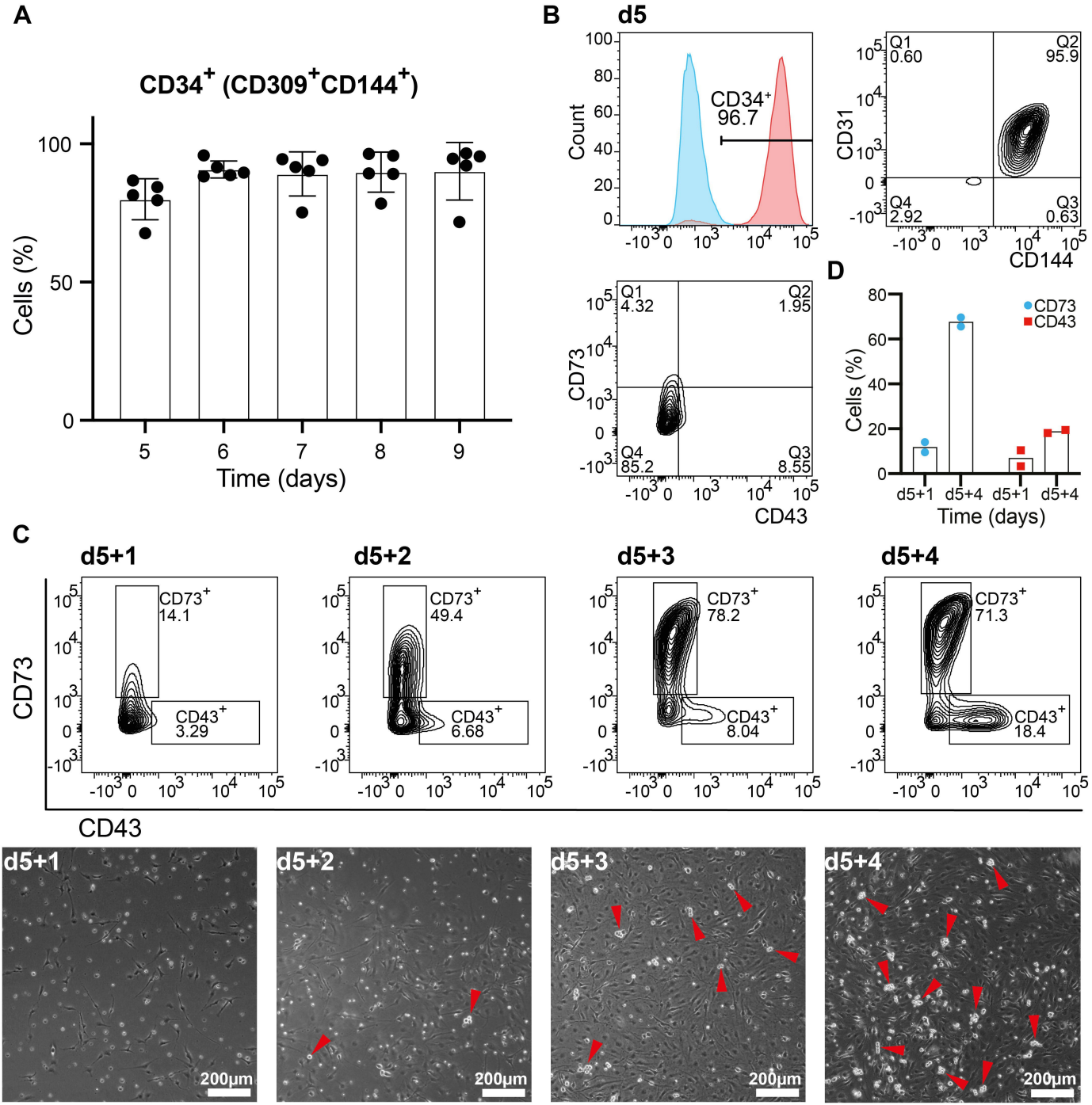
A
CD34+ (CD309+CD144+)
Cells (%)
Time (days)
B
d5
Count
CD34+
96.7
CD31
CD144
Q1
0.60
Q2
95.9
Q4
2.92
Q3
0.63
CD73
CD43
Q1
4.32
Q2
1.95
Q4
85.2
Q3
8.55
D
CD73
CD43
Cells (%)
d5+1
d5+4
d5+1
d5+4
Time (days)
C
d5+1
d5+2
d5+3
d5+4
CD73+
14.1
CD43+
3.29
CD73+
49.4
CD43+
6.68
CD73+
78.2
CD43+
8.04
CD73+
71.3
CD43+
18.4
CD73
CD43
d5+1
d5+2
d5+3
d5+4
200μm
200μm
200μm
200μm

Figure 2

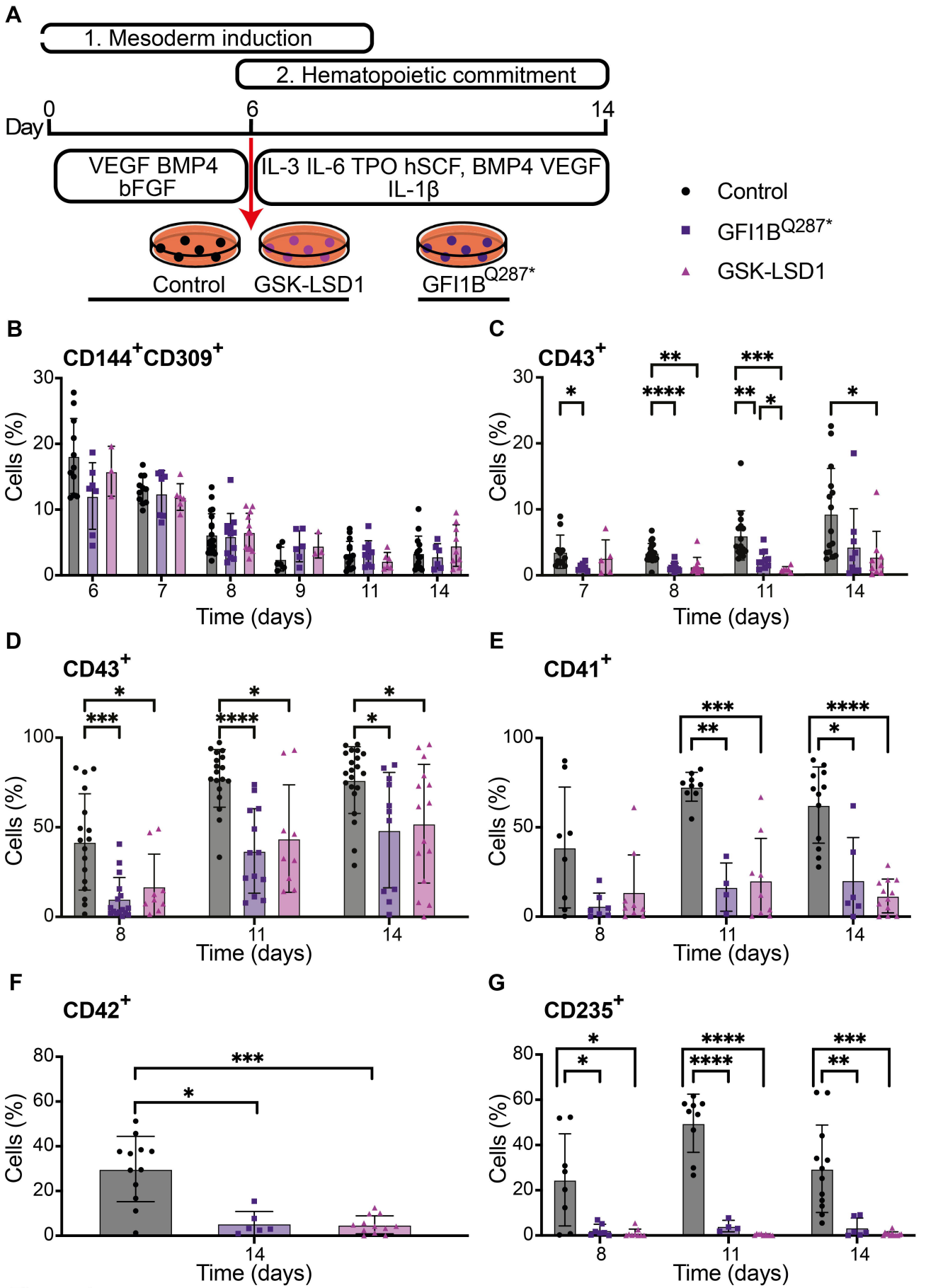
A
1. Mesoderm induction
2. Hematopoietic commitment
Day
0
6
14
VEGF BMP4 bFGF
IL-3 IL-6 TPO hSCF, BMP4 VEGF IL-1β
Control
GSK-LSD1
GFI1B^Q287*
Control
GFI1B^Q287*
GSK-LSD1
B
CD144+CD309+
Cells (%)
Time (days)
C
CD43+
Cells (%)
Time (days)
D
CD43+
Cells (%)
Time (days)
E
CD41+
Cells (%)
Time (days)
F
CD42+
Cells (%)
Time (days)
G
CD235+
Cells (%)
Time (days)

Figure 3

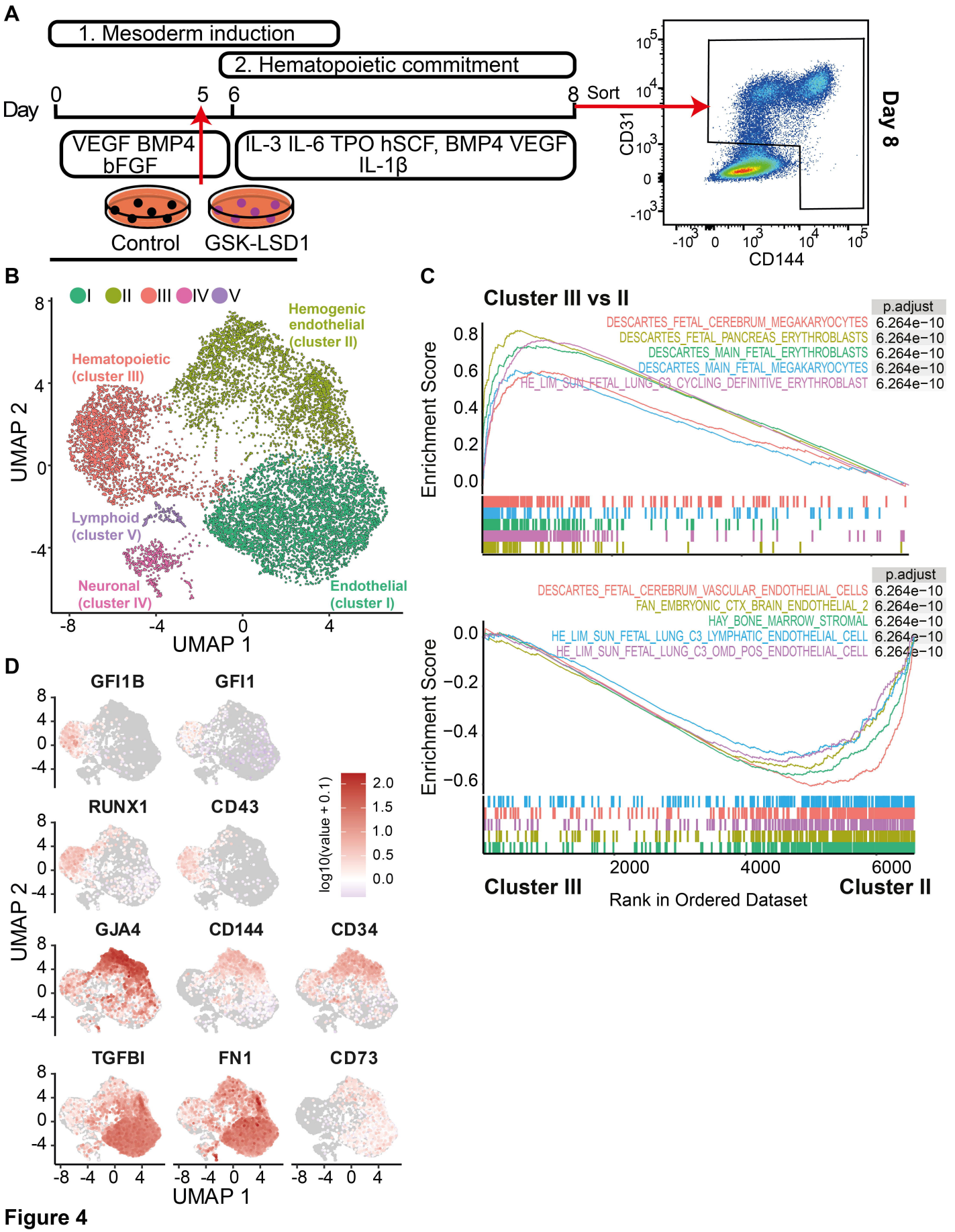
A
1. Mesoderm induction
2. Hematopoietic commitment
Day
0
5
6
8
Sort
VEGF BMP4 bFGF
IL-3 IL-6 TPO hSCF, BMP4 VEGF IL-1β
Control
GSK-LSD1
CD31
CD144
Day 8
B
I
II
III
IV
V
Hemogenic endothelial (cluster II)
Hematopoietic (cluster III)
Lymphoid (cluster V)
Neuronal (cluster IV)
Endothelial (cluster I)
UMAP 1
UMAP 2
C
Cluster III vs II
p.adjust
DESCARTES_FETAL_CEREBRUM_MEGAKARYOCYTES 6.264e−10
DESCARTES_FETAL_PANCREAS_ERYTHROBLASTS 6.264e−10
DESCARTES_MAIN_FETAL_ERYTHROBLASTS 6.264e−10
DESCARTES_MAIN_FETAL_MEGAKARYOCYTES 6.264e−10
HE_LIM_SUN_FETAL_LUNG_C3_CYCLING_DEFINITIVE_ERYTHROBLAST 6.264e−10
Enrichment Score
p.adjust
DESCARTES_FETAL_CEREBRUM_VASCULAR_ENDOTHELIAL_CELLS 6.264e−10
FAN_EMBRYONIC_CTX_BRAIN_ENDOTHELIAL_2 6.264e−10
HAY_BONE_MARROW_STROMAL 6.264e−10
HE_LIM_SUN_FETAL_LUNG_C3_LYMPHATIC_ENDOTHELIAL_CELL 6.264e−10
HE_LIM_SUN_FETAL_LUNG_C3_OMD_POS_ENDOTHELIAL_CELL 6.264e−10
Enrichment Score
Cluster III
Rank in Ordered Dataset
Cluster II
D
GFI1B
GFI1
RUNX1
CD43
GJA4
CD144
CD34
TGFBI
FN1
CD73
log10(value + 0.1)
UMAP 1
UMAP 2

Figure 4

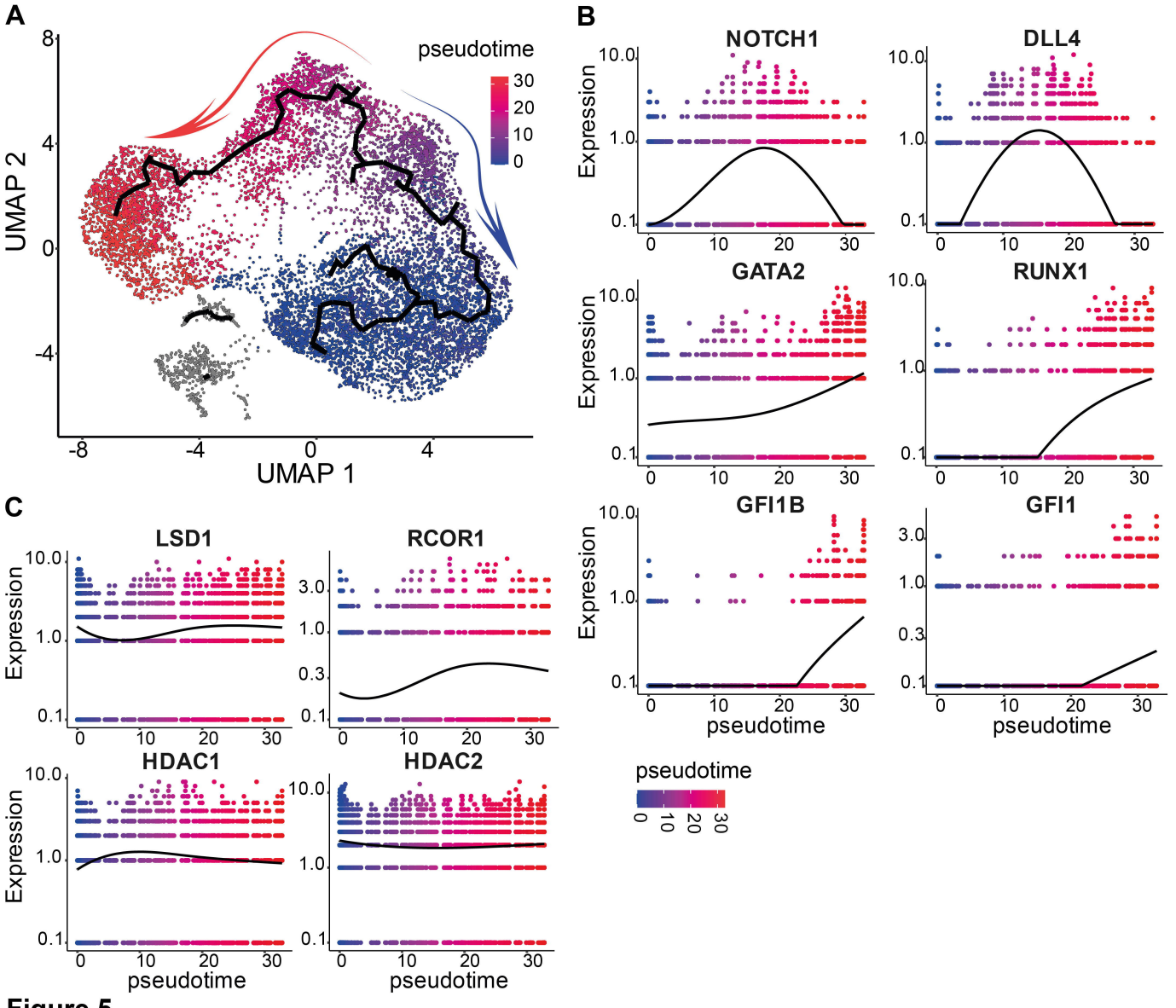
A
pseudotime
30
20
10
0
UMAP 2
UMAP 1
B
NOTCH1
DLL4
GATA2
RUNX1
GFI1B
GFI1
Expression
pseudotime
C
LSD1
RCOR1
HDAC1
HDAC2

Figure 5

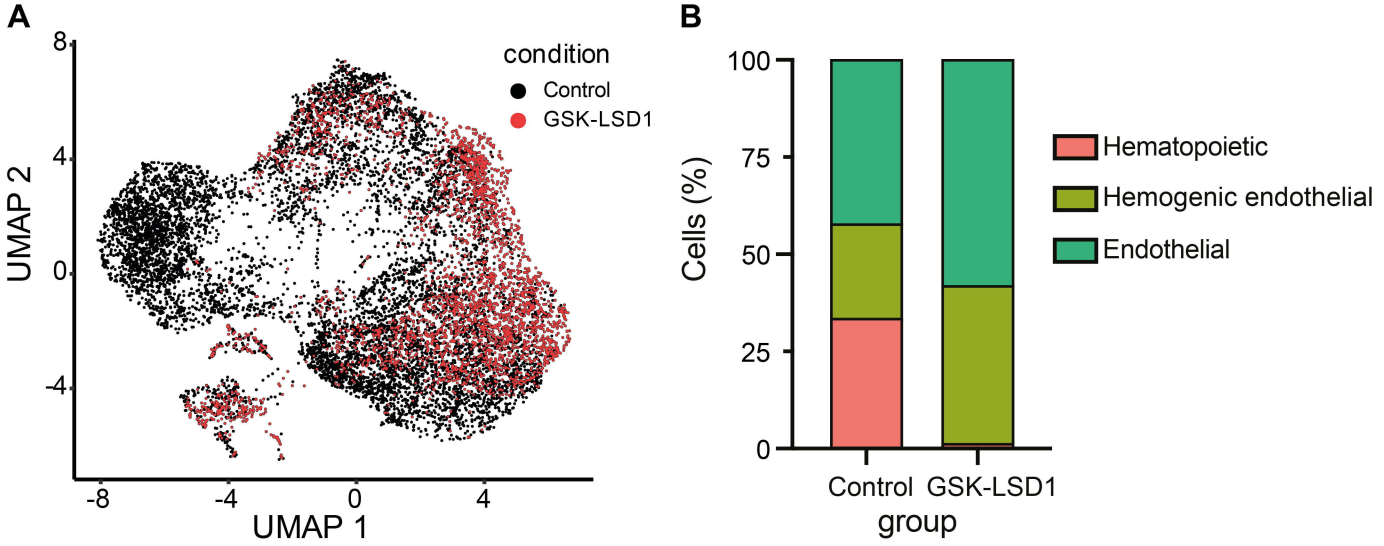
A
condition
Control
GSK-LSD1
UMAP 2
UMAP 1
8
4
0
-4
-8
-4
0
4
B
Cells (%)
100
75
50
25
0
Hematopoietic
Hemogenic endothelial
Endothelial
Control
GSK-LSD1
group

Figure 6

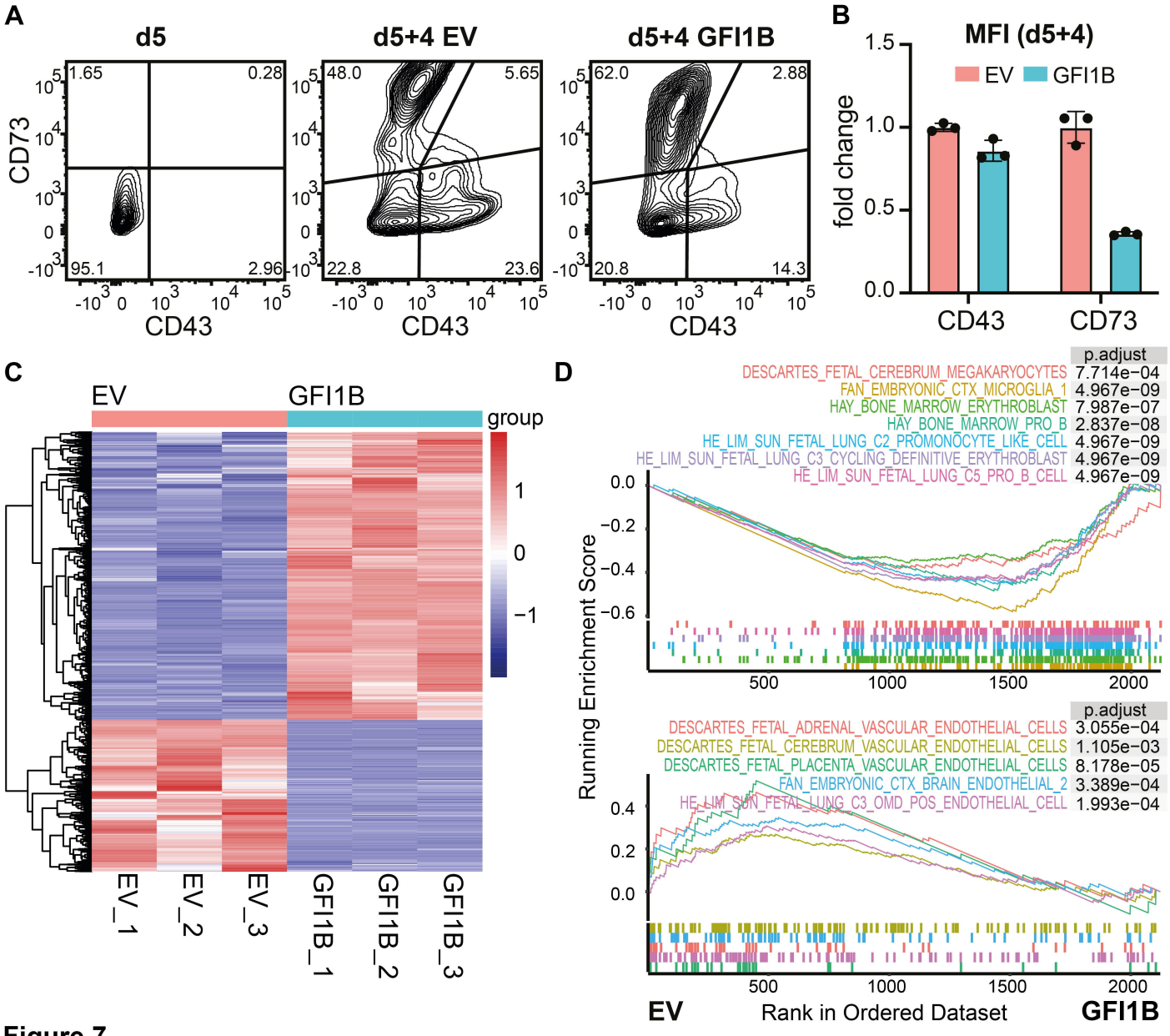
A
d5
d5+4 EV
d5+4 GFI1B
CD73
CD43
1.65
0.28
95.1
2.96
48.0
5.65
22.8
23.6
62.0
2.88
20.8
14.3
B
MFI (d5+4)
EV
GFI1B
fold change
CD43
CD73
C
EV
GFI1B
group
EV_1
EV_2
EV_3
GFI1B_1
GFI1B_2
GFI1B_3
D
p.adjust
DESCARTES_FETAL_CEREBRUM_MEGAKARYOCYTES 7.714e−04
FAN_EMBRYONIC_CTX_MICROGLIA_1 4.967e−09
HAY_BONE_MARROW_ERYTHROBLAST 7.987e−07
HAY_BONE_MARROW_PRO_B 2.837e−08
HE_LIM_SUN_FETAL_LUNG_C2_PROMONOCYTE_LIKE_CELL 4.967e−09
HE_LIM_SUN_FETAL_LUNG_C3_CYCLING_DEFINITIVE_ERYTHROBLAST 4.967e−09
HE_LIM_SUN_FETAL_LUNG_C5_PRO_B_CELL 4.967e−09
Running Enrichment Score
p.adjust
DESCARTES_FETAL_ADRENAL_VASCULAR_ENDOTHELIAL_CELLS 3.055e−04
DESCARTES_FETAL_CEREBRUM_VASCULAR_ENDOTHELIAL_CELLS 1.105e−03
DESCARTES_FETAL_PLACENTA_VASCULAR_ENDOTHELIAL_CELLS 8.178e−05
FAN_EMBRYONIC_CTX_BRAIN_ENDOTHELIAL_2 3.389e−04
HE_LIM_SUN_FETAL_LUNG_C3_OMD_POS_ENDOTHELIAL_CELL 1.993e−04
EV
Rank in Ordered Dataset
GFI1B

Figure 7

Supplementary Methods

iPSC lines:

The following iPSC lines were utilized in this study: MML-6838-cl2, SANi001-A, SANi002-A, all derived from a healthy donor, and two unique clones - SANi005-A and BEL-5-Cl.2, each containing a dominant negative GFI1B mutation ($GFI1B^{Q287*}$)[1–4]. The control iPSC lines (MML-6838-cl2, SANi001-A, SANi002-A) were subjected to LSD1 inhibition. The iPSC line MML-6838-cl2 was chosen for HE culture, GFI1B overexpression and single-cell RNA sequencing (scRNAseq) experiments.

Generation of *GFI1B* lentiviral construct

The wild type GFI1B coding sequence, complete with a preceding Kozak sequence and an XbaI restriction site, as well as a following BamHI restriction site (gBlocks from IDT), was cloned into the pJET1.2 vector using the CloneJET PCR Cloning Kit (ThermoFisher Scientific). After transformation, plasmids were isolated and digested with XbaI and BamHI. The band corresponding to the size of GFI1B was visualized on an agarose gel, after which it was subsequently purified and inserted into the LentiCRISPRv2GFP vector (Addgene #82416) following the excision of the Cas9 sequence using XbaI and BamHI. For the creation of an empty vector (EV) control, a double-stranded DNA sequence with overhangs of XbaI and BamHI, was inserted into the LentiCRISPRv2GFP vector to replace the Cas9 sequence cut by XbaI and BamHI.

Flow cytometry and sort

For flow cytometry experiments of the differentiating iPSC colonies, supernatant was harvested into a separate tube and attached cells on the plate were washed 2x with PBS before treatment for 5 minutes with TryplE Select. Cells were collected and passed through a 70µm cell strainer (NUNC) into a 50ml tube containing 10ml of IMDM with 20% FCS and washed with PBS. Both cells from the supernatant and the plate were stained with antibodies (Supplemental Table 1) for 30 minutes. They were then washed with FACS buffer (PBS+0.1% BSA+0.5mM EDTA) and analyzed using the LSD-II (BD Bioscience). For flow cytometry of HE cultures and transduction, cells were stained with CD43 and CD73 antibodies (Supplemental Table 1) and analyzed on FACSymphony™ A5 (BD Bioscience). For scRNAseq, sorting was performed with the BD FACSAria III (BD Bioscience) at room temperature after which cells were washed 3x with chilled DPBS and fixated with 80% chilled methanol. Cells were incubated for 20 minutes at -20°C after which they were submitted for scRNAseq. For outgrowth experiments (Supplemental Fig. 1A), $CD144^{+}CD309^{+}$ cells with either CD73 or CD43 positivity were sorted on day 8 of differentiation and cultured in day 6 iPSC differentiation media for an addition 5 days on cell culture treated plates. FlowJo was used for flow cytometry data analysis.

Reference:

1. Hansen M, Varga E, Wüst T, et al. Generation and characterization of human iPSC line MML-6838-Cl2 from mobilized peripheral blood derived megakaryoblasts. Stem Cell Res. 2017;18:26–28.
2. Hansen M, Varga E, Wüst T, et al. Generation and characterization of human iPSC lines SANi001-A and SANi002-A from mobilized peripheral blood derived megakaryoblasts. Stem Cell Res. 2017;25:42–45.
3. Hansen M, Varga E, Wüst T, et al. Generation and characterization of a human iPSC line SANi005-A containing the gray platelet associated heterozygous mutation p.Q287* in GFI1B. Stem Cell Res. 2017;25:34–37.
4. Van Oorschot R, Hansen M, Koornneef JM, et al. Molecular mechanisms of bleeding disorderassociated GFI1BQ287* mutation and its affected pathways in megakaryocytes and platelets. Haematologica. 2019;104(7):1460.

Supplemental Table 1. antibodies used in this study.

Product	Conjugate	Manufacturer	Dilution	Clone	Cat#
CD34	APC	Biolegend	1:500	581	343510
CD34	BV510	Biolegend	1:300	581	343528
CD31	APC-eF780	eBioscience	1:800	WM-59	47-031942
CD144	FITC	BD	1:100	55-7H1	560411
CD309	PE	Miltenyi	1:800	ES8-20E6	130-093-598
CD41	PE-Cy7	Biolegend	1:1000	HIP8	303718
CD41	Pacific Blue	Biolegend	1:100	HIP8	303714
CD43	PE-Cy7	Biolegend	1:200	CD43-10G7	343208
CD235	PE	Acris	1:2500	JC159	DM066R
CD42	FITC	Diaclone	1:50	HIP1	853.231.010
CD73	APC	Biolegend	1:100	AD2	344006

Supplemental Table 2. Analysis of day 8 CD144$^+$/CD31$^+$ scRNAseq data. (A) Modules of genes differentially expressed between clusters in Fig. 4B. **(B)** Cell types predicted from gene modules in A. **(C)** Differential gene expression between cluster III and cluster II in Fig. 4B. **(D)** GSEA result of C8 cell type gene sets for differentially expressed genes between cluster III and II in Fig. 4B. **(E)** GSEA result of C2 curated gene sets for differentially expressed genes between cluster III and II in Fig. 4B. **(F)** Differential gene expression between cluster II and cluster I in Fig. 4B. **(G)** GSEA result of C8 cell type gene sets for differentially expressed genes between cluster II and I in Fig. 4B. (see excel file)

https://1drv.ms/x/c/96eafeebb0308bd4/EaQ-PDG_RR9EihOyVoma9CEBOyNz5QhcPvWDsrcS1eoL1A

Supplemental Table 3. Bulk RNAseq analysis of EV/GFI1B ectopically expressed CD34$^+$ iPSC-HE. (A) Differential gene expression results between the EV and GFI1B groups on day 4 following transduction. **(B)** Gene Ontology results for differentially expressed genes between the EV and GFI1B groups. **(C)** GSEA result of C8 cell type gene sets for differentially expressed genes between the EV and GFI1B groups. (see excel file)

https://1drv.ms/x/c/96eafeebb0308bd4/EVUgEfWpOR1OspPrLmCjNR0Bp70zyZfjjyQv2MFguSh5kQ

Supplemental Fig.1. GFI1B and LSD1 affect hematopoietic and endothelial specification from hematopoietic/endothelial precursors. (A) CD144$^+$CD309$^+$ cells (left flow plot) were sorted based on the expression of CD73 and CD43 (middle flow plot). These cells were reseeded and cultured for five days. Images on the right, photographed using the EVOS-XL core, 4x objective, are a representative of day 8 sorted cells after five days of culturing. Note the presence of endothelial like adherent cells in the CD144$^+$CD309$^+$CD73$^+$ cultured population and nonadherent hematopoietic blasts in the CD144$^+$CD309$^+$CD41$^+$ cultured population. **(B)** The percentage of CD73$^+$ cells in CD31$^+$ population within the differentiated iPSC colonies (n=8-9 for control, 5-7 for GFI1B^{Q287*}, and 3 for GSK-LSD1). Data represent mean +/- SD, analyzed using two-way ANOVA, Tukey's multiple comparisons test. Significance levels: * < 0.05, ** <0.005, *** <0.0005, **** <0.00005. Representations: Black circles = control iPSC; Red triangles = iPSC treated with GSK-LSD1 inhibitor; Purple squares = GFI1B^{Q287*} iPSC. **(C)** Absolute number of suspension cells in paired control (filled circle) and GFI1B^{Q287*} (purple square) cultures. **(D)** Absolute number of suspension cells in paired control (filled circle) and GSK-LSD1 (red triangle) treated cultures. **(E)** Percentage of CD43$^+$/CD73$^+$ cells within the CD144$^+$/CD31$^+$ population from day 5 to day 9 of iPSC differentiation (mean +/- SD; n=5). Representative flow plot for day 8 shown on the left.

Supplemental Fig.2. Genes and gene modules used to identify CD31$^+$/CD144$^+$ populations. (A) Heatmap displaying scaled expression of gene modules, grouped based on differentially expressed genes identified between clusters from CD31$^+$/CD144$^+$ single cell data (Fig. 4B). **(B)** The expression of gene modules 3, 5, 8, 9, 10, and 11 on UMAP. **(C)** Gene set enrichment plot depicting highly enriched expression of genes involved in hematopoietic stem cell function in cluster II compared to cluster III. **(D)** Enrichment of hematopoietic cell types in cluster II (top plot) and endothelial cell types in cluster I (bottom plot) by gene set enrichment analysis (GSEA).

Supplemental Fig.3. Marker genes expression in CD31$^+$/CD144$^+$ clusters. Dot plot showing the scaled expression of top 15 differentially expressed genes from every cluster depicted in Fig. 4B.

Supplemental Fig.4. Genes expression on UMAP of CD31$^+$/CD144$^+$ populations. The expression of hematopoietic (first row), hemogenic endothelial (second row), endothelial (third row), lymphoid (CD3E, CD3G, CD7), and neuronal (PTPRZ1, SOX2) cluster specific genes on UMAP.

Supplemental Fig.5. The presence of known EHT regulators and GFI1B cofactors in iPSC-HE. (A) Expression of *LCOR*, *ERG*, *SPI1*, *HOXA5*, and *HOXA9* over pseudotime. **(B)** Expression of *LCOR*, *ERG*, *SPI1*, *HOXA5*, and *HOXA9* on UMAP. **(C)** Expression of known GFI1B cofactors on UMAP. Note their presence in the hemogenic endothelial population (Fig. 4B).

Supplemental Fig.6. LSD1 inhibition results in the absence of hematopoietic population in CD31$^+$/CD144$^+$ single cell data. Total number of cells in the hematopoietic, hemogenic endothelial (HE), and endothelial clusters from Fig. 4B for both control (in black) and GSK-LSD1 treated conditions (in red).

Supplemental Fig.7. Overexpression of GFI1B in CD34$^+$ iPSC-HE increases cell proliferation. (A) Integration of day 5 and day 8 sorted CD144$^+$/CD31$^+$ single cells on UMAP. **(B)** Expression of *GFI1B* and *LSD1* on UMAP of day 5 and day 8 integrated CD144$^+$/CD31$^+$ cells. **(C)** Percentage of GFP positive cells at day 5 after lentiviral transduction on day 5 sorted CD34$^+$ iPSC-HE cells (d5+5). Total number of **(D)** all cells, **(E)** CD43$^+$ and CD73$^+$ cells, in the empty vector (EV) and the GFI1B overexpressed CD34$^+$ iPSC-HE, counted after 4 days of transduction. **(D-E)** Data represent three independent experiments with mean +/- SD. Mann-Whitney tests were performed, with p = 0.1 for all. EV condition is shown red, and GFI1B condition is shown in blue.

Supplemental Fig.8. Ectopic expression of GFI1B in iPSC-HE upregulates hematopoietic genes and downregulates endothelial genes. (A) Principal component (PC) analysis of RNA sequencing data from day 4 transduced hemogenic endothelium. PC1 and PC2 account for 76% and 11% of the variance separately. **(B)** Volcano plot displaying differentially expressed genes (DEGs) in the GFI1B overexpressed HE comparing to the EV group. Threshold for log2FC and p value are set at 1 and 0.01 respectively. Upregulated genes are colored in red and downregulated in blue. Names of the top 10 DEGs are highlighted. **(C)** Normalized CPM (count per million) of *GFI1*, *GFI1B*, *HOXA9*, *HOXA10*, *CD43*, *GATA2*, *RUNX1*, *CD73*, and *SOX17* for both the EV and GFI1B overexpressed CD34$^+$ iPSC-HE.

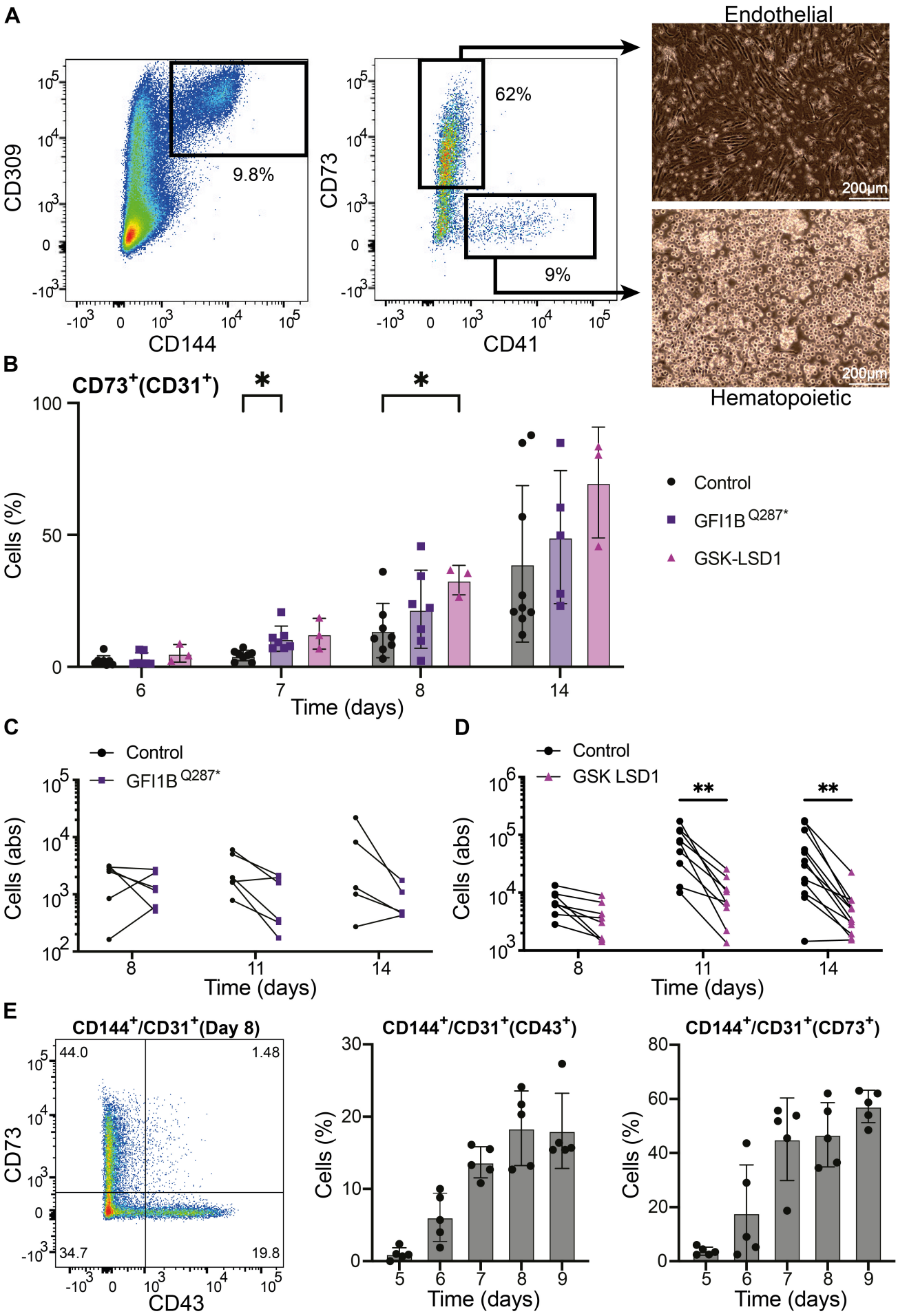

Supplemental Figure 1

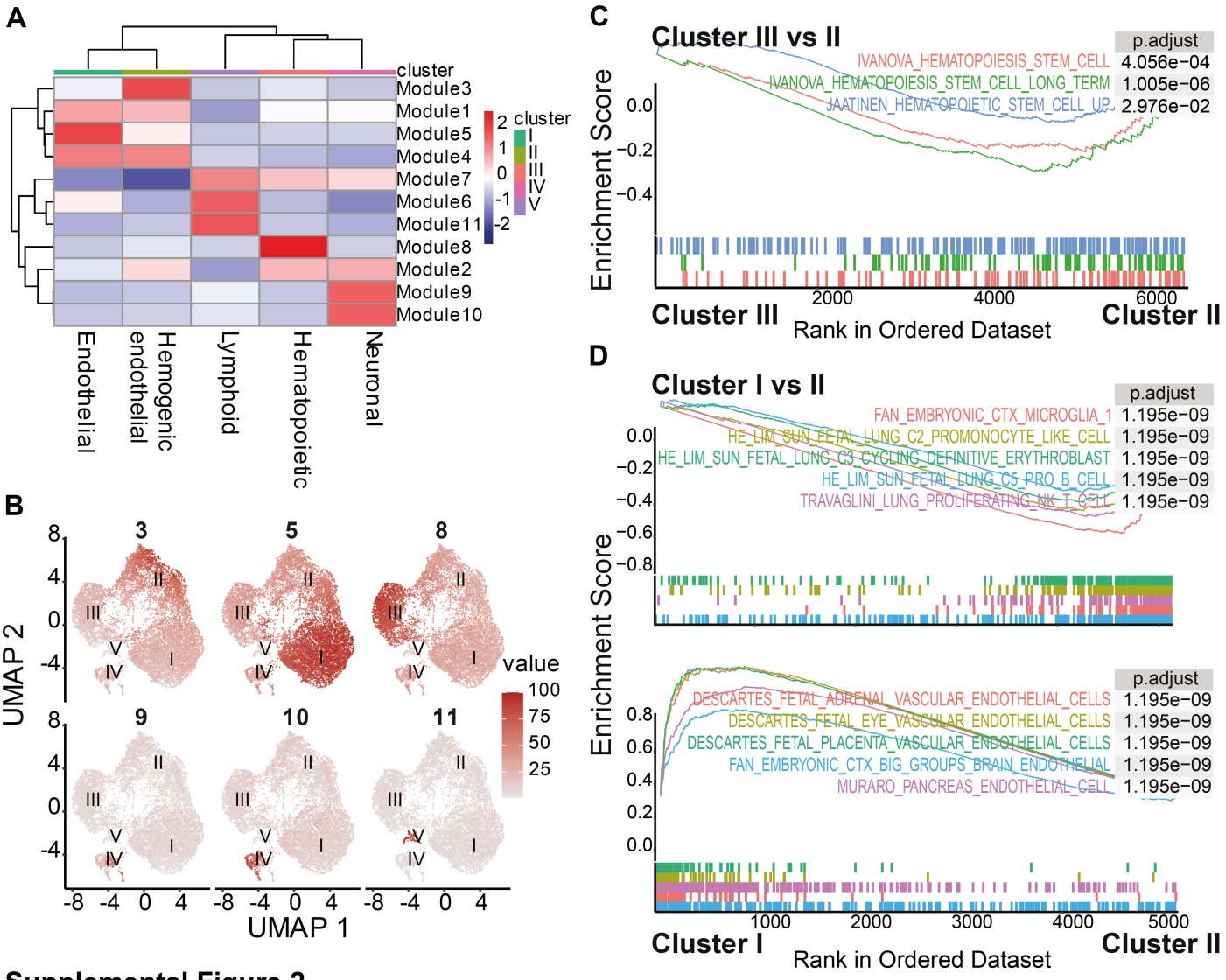

Supplemental Figure 2

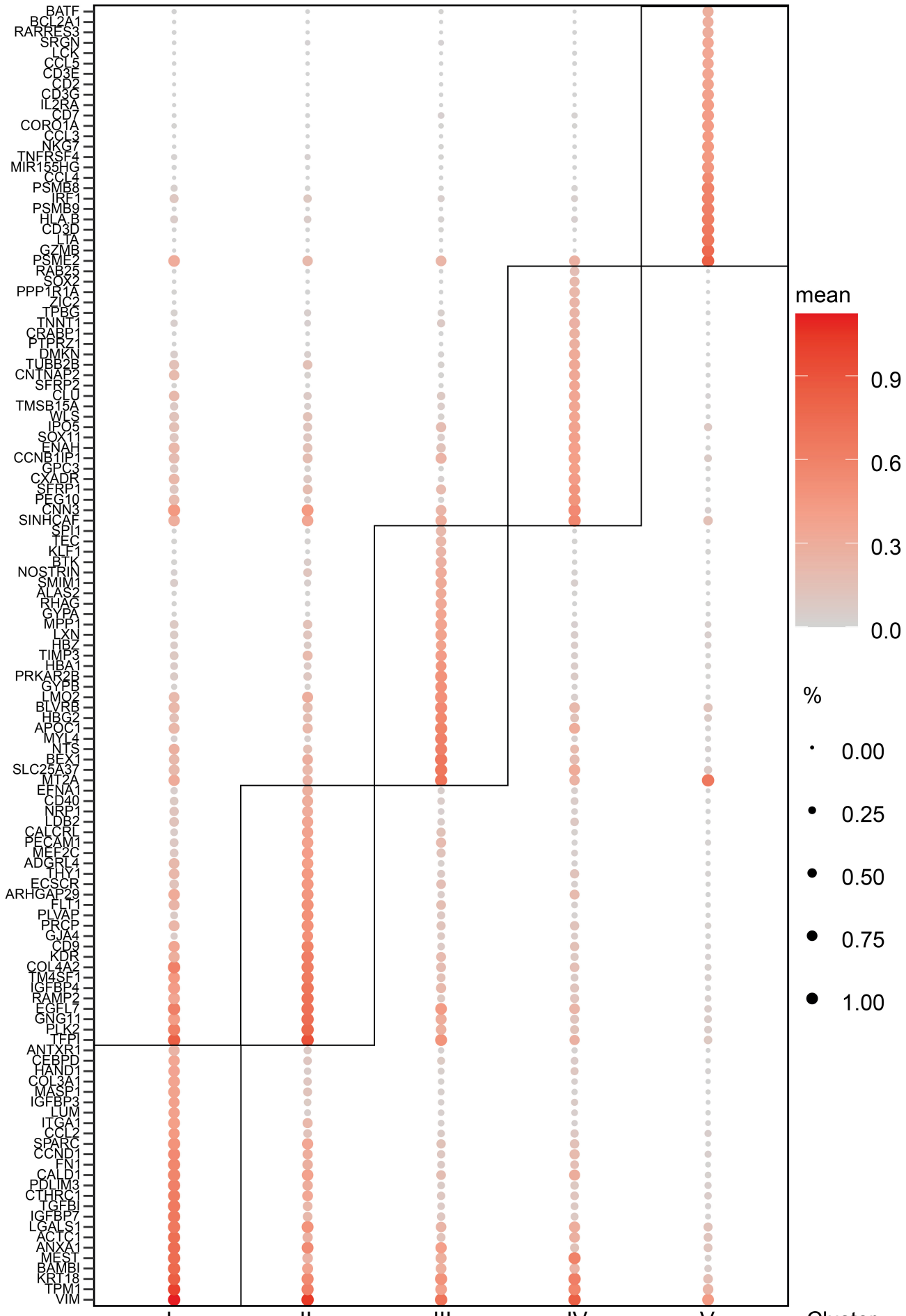

Supplemental Figure 3

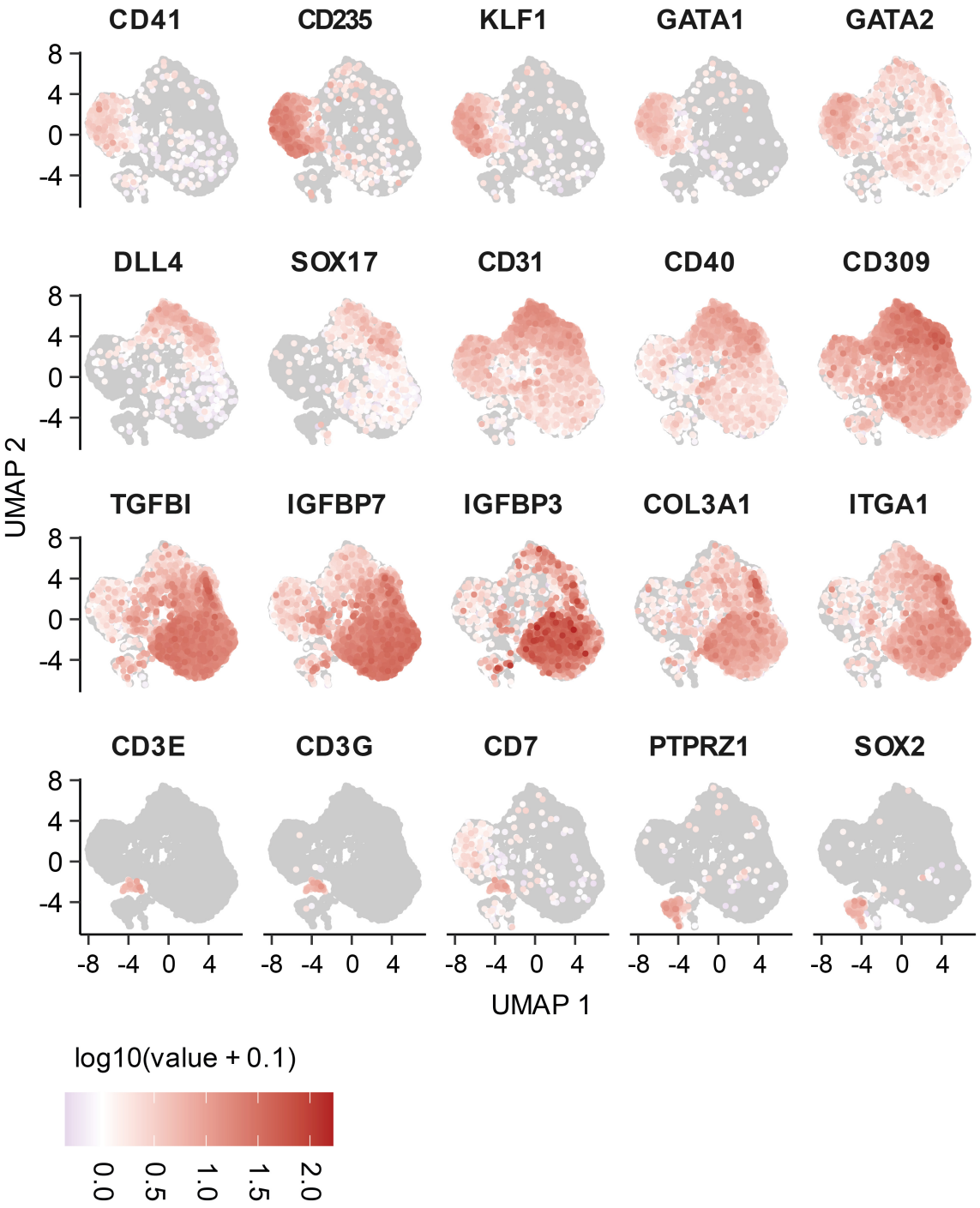

Supplemental Figure 4

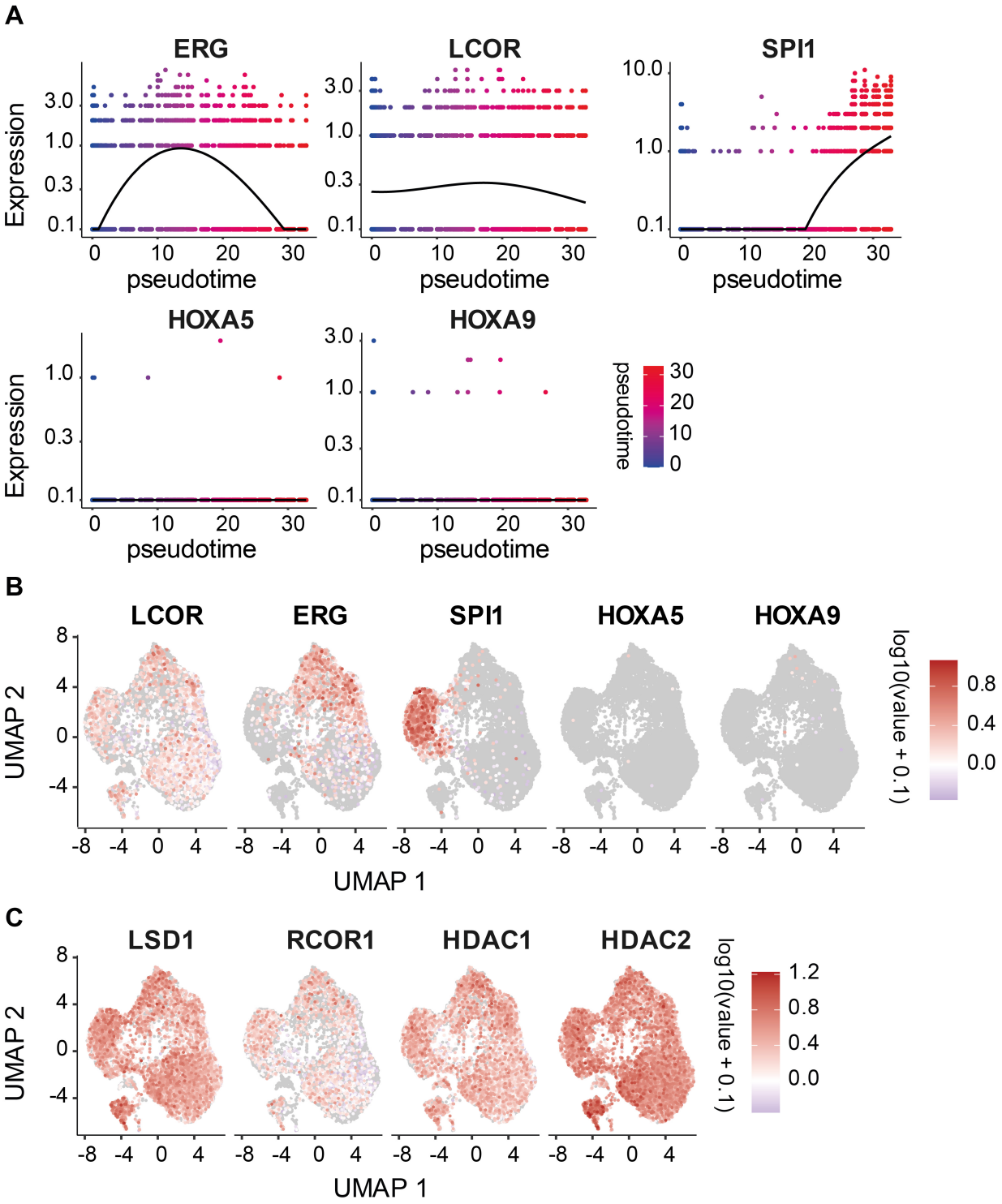

Supplemental Figure 5

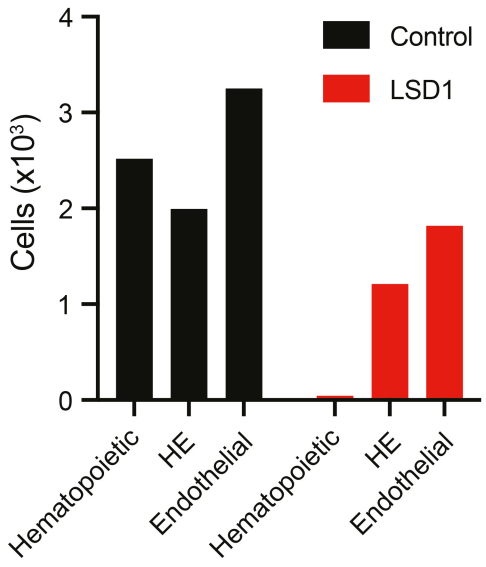

Supplemental Figure 6

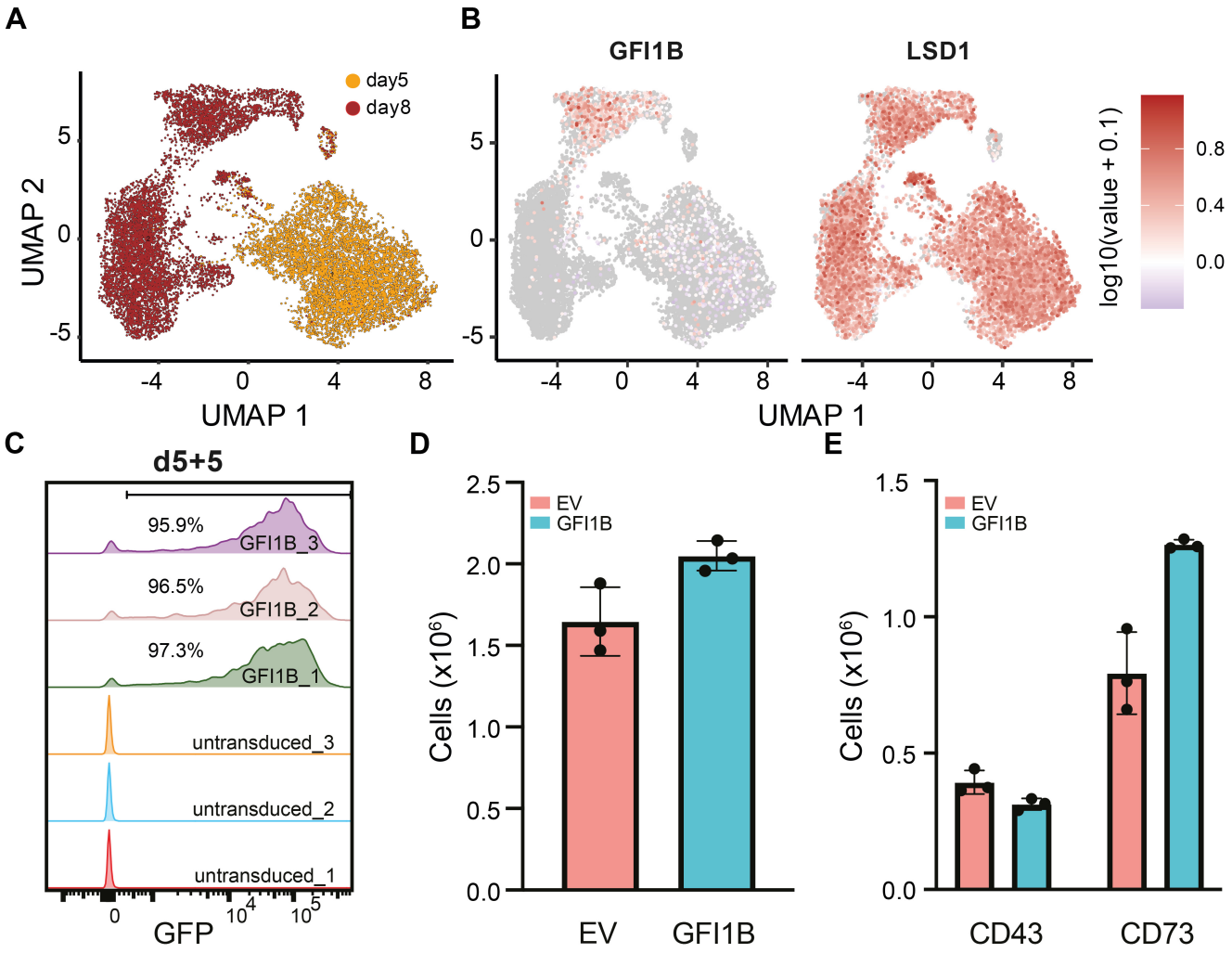

Supplemental Figure 7

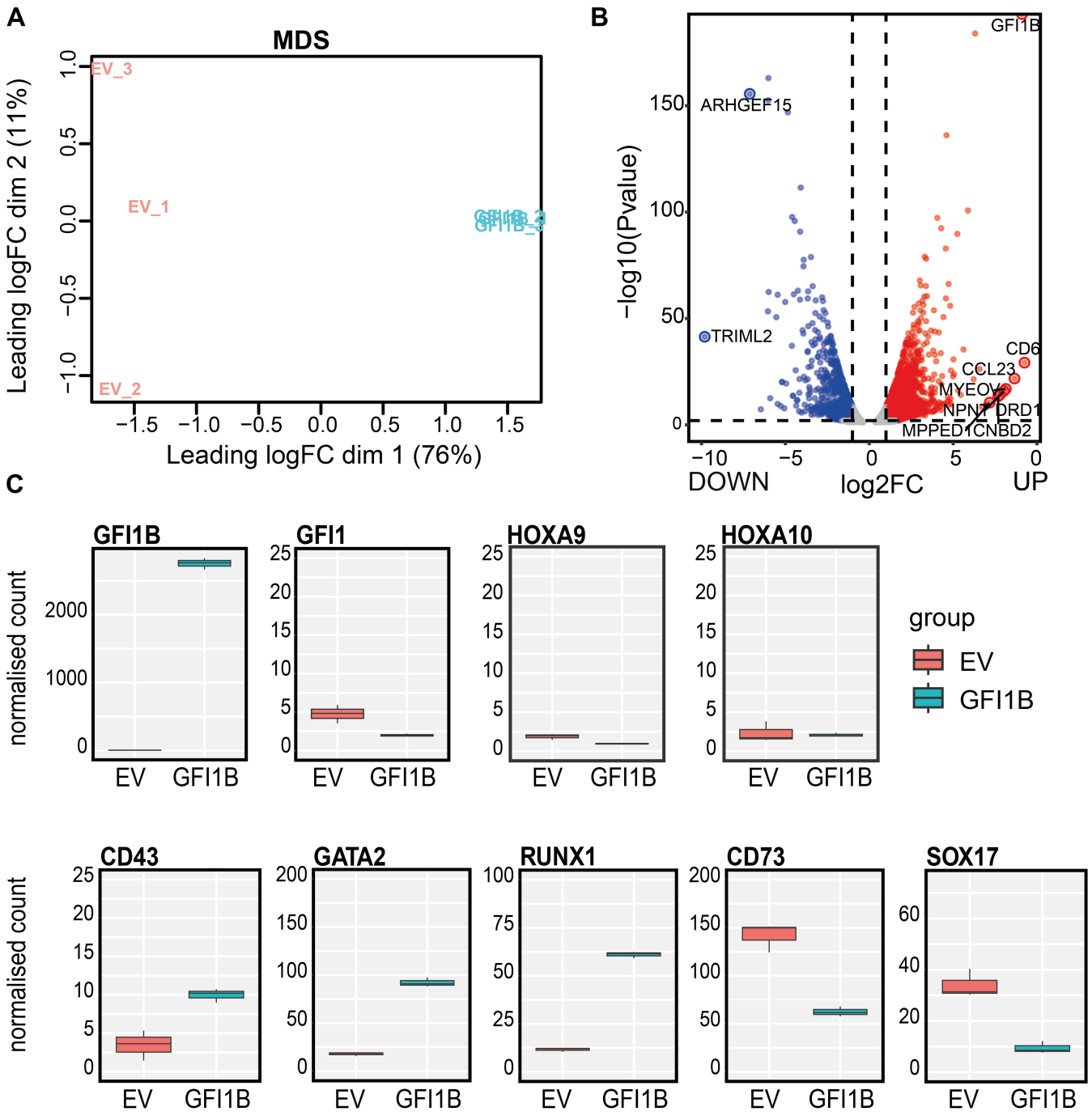

Supplemental Figure 8